

Measurement of the CKM Matrix Element $|V_{cb}|$ from $B^0 \rightarrow D^{*-} \ell^+ \nu_\ell$ at Belle

E. Waheed,⁵¹ P. Urquijo,⁵¹ I. Adachi,^{18, 14} K. Adamczyk,⁶³ H. Aihara,⁸⁷ S. Al Said,^{81, 36} D. M. Asner,⁴ H. Atmacan,⁷⁸ T. Aushev,⁵⁵ R. Ayad,⁸¹ V. Babu,⁸² I. Badhrees,^{81, 35} V. Bansal,⁶⁹ P. Behera,²⁴ C. Beleno,¹³ F. Bernlochner,³ B. Bhuyan,²² T. Bilka,⁶ J. Biswal,³² A. Bobrov,^{5, 67} G. Bonvicini,⁹¹ A. Bozek,⁶³ M. Bračko,^{49, 32} T. E. Browder,¹⁷ M. Campajola,^{29, 58} D. Červenkov,⁶ P. Chang,⁶² V. Chekelian,⁵⁰ A. Chen,⁶⁰ B. G. Cheon,¹⁶ K. Chilikin,⁴⁴ H. E. Cho,¹⁶ K. Cho,³⁸ S.-K. Choi,¹⁵ Y. Choi,⁷⁹ S. Choudhury,²³ D. Cinabro,⁹¹ S. Cunliffe,⁹ S. Di Carlo,⁴² Z. Doležal,⁶ T. V. Dong,^{18, 14} D. Dossett,⁵¹ S. Eidelman,^{5, 67, 44} D. Epifanov,^{5, 67} J. E. Fast,⁶⁹ B. G. Fulson,⁶⁹ R. Garg,⁷⁰ V. Gaur,⁹⁰ A. Garmash,^{5, 67} A. Giri,²³ P. Goldenzweig,³³ B. Golob,^{46, 32} O. Grzymkowska,⁶³ J. Haba,^{18, 14} T. Hara,^{18, 14} K. Hayasaka,⁶⁵ H. Hayashii,⁵⁹ M. T. Hedges,¹⁷ W.-S. Hou,⁶² C.-L. Hsu,⁸⁰ T. Iijima,^{57, 56} K. Inami,⁵⁶ G. Inguglia,²⁷ A. Ishikawa,⁸⁵ M. Iwasaki,⁶⁸ Y. Iwasaki,¹⁸ W. W. Jacobs,²⁵ H. B. Jeon,⁴¹ S. Jia,² Y. Jin,⁸⁷ D. Joffe,³⁴ K. K. Joo,⁷ J. Kahn,⁴⁷ A. B. Kaliyar,²⁴ G. Karyan,⁹ T. Kawasaki,³⁷ C. H. Kim,¹⁶ D. Y. Kim,⁷⁷ K. T. Kim,³⁹ S. H. Kim,¹⁶ K. Kinoshita,⁸ P. Kodyš,⁶ S. Korpar,^{49, 32} D. Kotchetkov,¹⁷ P. Križan,^{46, 32} R. Kroeger,⁵² P. Krokovny,^{5, 67} T. Kuhr,⁴⁷ R. Kulasiri,³⁴ A. Kuzmin,^{5, 67} Y.-J. Kwon,⁹³ J. S. Lange,¹² J. Y. Lee,⁷⁵ S. C. Lee,⁴¹ C. H. Li,⁴⁵ L. K. Li,²⁶ Y. B. Li,⁷¹ L. Li Gioi,⁵⁰ J. Libby,²⁴ K. Lieret,⁴⁷ D. Liventsev,^{90, 18} P.-C. Lu,⁶² T. Luo,¹¹ J. MacNaughton,⁵³ M. Masuda,⁸⁶ D. Matvienko,^{5, 67, 44} M. Merola,^{29, 58} F. Metzner,³³ K. Miyabayashi,⁵⁹ H. Miyata,⁶⁵ R. Mizuk,^{44, 54, 55} G. B. Mohanty,⁸² T. Mori,⁵⁶ R. Mussa,³⁰ I. Nakamura,^{18, 14} M. Nakao,^{18, 14} K. J. Nath,²² Z. Natkaniec,⁶³ M. Nayak,^{91, 18} M. Niyyama,⁴⁰ N. K. Nisar,⁷² S. Nishida,^{18, 14} K. Nishimura,¹⁷ S. Ogawa,⁸⁴ H. Ono,^{64, 65} P. Pakhlov,^{44, 54} G. Pakhlova,^{44, 55} B. Pal,⁴ S. Pardi,²⁹ H. Park,⁴¹ S.-H. Park,⁹³ S. Paul,⁸³ R. Pestotnik,³² L. E. Piilonen,⁹⁰ V. Popov,^{44, 55} E. Prencipe,²⁰ M. Prim,³³ A. Rostomyan,⁹ G. Russo,²⁹ Y. Sakai,^{18, 14} M. Salehi,^{48, 47} S. Sandilya,⁸ T. Sanuki,⁸⁵ V. Savinov,⁷² O. Schneider,⁴³ G. Schnell,^{1, 21} J. Schueler,¹⁷ C. Schwanda,²⁷ Y. Seino,⁶⁵ K. Senyo,⁹² O. Seon,⁵⁶ M. E. Sevior,⁵¹ V. Shebalin,¹⁷ C. P. Shen,² J.-G. Shiu,⁶² B. Shwartz,^{5, 67} F. Simon,⁵⁰ A. Sokolov,²⁸ E. Solovieva,⁴⁴ S. Stanič,⁶⁶ M. Starič,³² Z. S. Stottler,⁹⁰ J. F. Strube,⁶⁹ T. Sumiyoshi,⁸⁹ M. Takizawa,^{76, 19, 73} K. Tanida,³¹ F. Tenchini,⁹ K. Trabelsi,⁴² M. Uchida,⁸⁸ T. Uglov,^{44, 55} Y. Unno,¹⁶ S. Uno,^{18, 14} Y. Usov,^{5, 67} G. Varner,¹⁷ K. E. Varvell,⁸⁰ A. Vinokurova,^{5, 67} A. Vossen,¹⁰ C. H. Wang,⁶¹ M.-Z. Wang,⁶² P. Wang,²⁶ E. Won,³⁹ S. B. Yang,³⁹ H. Ye,⁹ Y. Yusa,⁶⁵ Z. P. Zhang,⁷⁴ V. Zhilich,^{5, 67} and V. Zhukova⁴⁴

(The Belle Collaboration)

¹University of the Basque Country UPV/EHU, 48080 Bilbao

²Beihang University, Beijing 100191

³University of Bonn, 53115 Bonn

⁴Brookhaven National Laboratory, Upton, New York 11973

⁵Budker Institute of Nuclear Physics SB RAS, Novosibirsk 630090

⁶Faculty of Mathematics and Physics, Charles University, 121 16 Prague

⁷Chonnam National University, Kwangju 660-701

⁸University of Cincinnati, Cincinnati, Ohio 45221

⁹Deutsches Elektronen-Synchrotron, 22607 Hamburg

¹⁰Duke University, Durham, North Carolina 27708

¹¹Key Laboratory of Nuclear Physics and Ion-beam Application (MOE) and Institute of Modern Physics, Fudan University, Shanghai 200443

¹²Justus-Liebig-Universität Gießen, 35392 Gießen

¹³II. Physikalisches Institut, Georg-August-Universität Göttingen, 37073 Göttingen

¹⁴SOKENDAI (The Graduate University for Advanced Studies), Hayama 240-0193

¹⁵Gyeongsang National University, Chinju 660-701

¹⁶Hanyang University, Seoul 133-791

¹⁷University of Hawaii, Honolulu, Hawaii 96822

¹⁸High Energy Accelerator Research Organization (KEK), Tsukuba 305-0801

¹⁹J-PARC Branch, KEK Theory Center, High Energy Accelerator Research Organization (KEK), Tsukuba 305-0801

²⁰Forschungszentrum Jülich, 52425 Jülich

²¹IKERBASQUE, Basque Foundation for Science, 48013 Bilbao

²²Indian Institute of Technology Guwahati, Assam 781039

²³Indian Institute of Technology Hyderabad, Telangana 502285

²⁴Indian Institute of Technology Madras, Chennai 600036

²⁵Indiana University, Bloomington, Indiana 47408

²⁶Institute of High Energy Physics, Chinese Academy of Sciences, Beijing 100049

²⁷Institute of High Energy Physics, Vienna 1050

²⁸Institute for High Energy Physics, Protvino 142281

²⁹INFN - Sezione di Napoli, 80126 Napoli

- ³⁰INFN - Sezione di Torino, 10125 Torino
³¹Advanced Science Research Center, Japan Atomic Energy Agency, Naka 319-1195
³²J. Stefan Institute, 1000 Ljubljana
³³Institut für Experimentelle Teilchenphysik, Karlsruher Institut für Technologie, 76131 Karlsruhe
³⁴Kennesaw State University, Kennesaw, Georgia 30144
³⁵King Abdulaziz City for Science and Technology, Riyadh 11442
³⁶Department of Physics, Faculty of Science, King Abdulaziz University, Jeddah 21589
³⁷Kitasato University, Sagamihara 252-0373
³⁸Korea Institute of Science and Technology Information, Daejeon 305-806
³⁹Korea University, Seoul 136-713
⁴⁰Kyoto University, Kyoto 606-8502
⁴¹Kyungpook National University, Daegu 702-701
⁴²LAL, Univ. Paris-Sud, CNRS/IN2P3, Université Paris-Saclay, Orsay
⁴³École Polytechnique Fédérale de Lausanne (EPFL), Lausanne 1015
⁴⁴P.N. Lebedev Physical Institute of the Russian Academy of Sciences, Moscow 119991
⁴⁵Liaoning Normal University, Dalian 116029
⁴⁶Faculty of Mathematics and Physics, University of Ljubljana, 1000 Ljubljana
⁴⁷Ludwig Maximilians University, 80539 Munich
⁴⁸University of Malaya, 50603 Kuala Lumpur
⁴⁹University of Maribor, 2000 Maribor
⁵⁰Max-Planck-Institut für Physik, 80805 München
⁵¹School of Physics, University of Melbourne, Victoria 3010
⁵²University of Mississippi, University, Mississippi 38677
⁵³University of Miyazaki, Miyazaki 889-2192
⁵⁴Moscow Physical Engineering Institute, Moscow 115409
⁵⁵Moscow Institute of Physics and Technology, Moscow Region 141700
⁵⁶Graduate School of Science, Nagoya University, Nagoya 464-8602
⁵⁷Kobayashi-Maskawa Institute, Nagoya University, Nagoya 464-8602
⁵⁸Università di Napoli Federico II, 80055 Napoli
⁵⁹Nara Women's University, Nara 630-8506
⁶⁰National Central University, Chung-li 32054
⁶¹National United University, Miao Li 36003
⁶²Department of Physics, National Taiwan University, Taipei 10617
⁶³H. Niewodniczanski Institute of Nuclear Physics, Krakow 31-342
⁶⁴Nippon Dental University, Niigata 951-8580
⁶⁵Niigata University, Niigata 950-2181
⁶⁶University of Nova Gorica, 5000 Nova Gorica
⁶⁷Novosibirsk State University, Novosibirsk 630090
⁶⁸Osaka City University, Osaka 558-8585
⁶⁹Pacific Northwest National Laboratory, Richland, Washington 99352
⁷⁰Panjab University, Chandigarh 160014
⁷¹Peking University, Beijing 100871
⁷²University of Pittsburgh, Pittsburgh, Pennsylvania 15260
⁷³Theoretical Research Division, Nishina Center, RIKEN, Saitama 351-0198
⁷⁴University of Science and Technology of China, Hefei 230026
⁷⁵Seoul National University, Seoul 151-742
⁷⁶Showa Pharmaceutical University, Tokyo 194-8543
⁷⁷Soongsil University, Seoul 156-743
⁷⁸University of South Carolina, Columbia, South Carolina 29208
⁷⁹Sungkyunkwan University, Suwon 440-746
⁸⁰School of Physics, University of Sydney, New South Wales 2006
⁸¹Department of Physics, Faculty of Science, University of Tabuk, Tabuk 71451
⁸²Tata Institute of Fundamental Research, Mumbai 400005
⁸³Department of Physics, Technische Universität München, 85748 Garching
⁸⁴Toho University, Funabashi 274-8510
⁸⁵Department of Physics, Tohoku University, Sendai 980-8578
⁸⁶Earthquake Research Institute, University of Tokyo, Tokyo 113-0032
⁸⁷Department of Physics, University of Tokyo, Tokyo 113-0033
⁸⁸Tokyo Institute of Technology, Tokyo 152-8550
⁸⁹Tokyo Metropolitan University, Tokyo 192-0397
⁹⁰Virginia Polytechnic Institute and State University, Blacksburg, Virginia 24061
⁹¹Wayne State University, Detroit, Michigan 48202
⁹²Yamagata University, Yamagata 990-8560

⁹³ Yonsei University, Seoul 120-749

We present a new measurement of the CKM matrix element $|V_{cb}|$ from $B^0 \rightarrow D^{*-} \ell^+ \nu_\ell$ decays, reconstructed with the full Belle data set of 711 fb^{-1} integrated luminosity. Two form factor parameterizations, originally conceived by the Caprini-Lellouch-Neubert (CLN) and the Boyd, Grinstein and Lebed (BGL) groups, are used to extract the product $\mathcal{F}(1)\eta_{\text{EW}}|V_{cb}|$ and the decay form factors, where $\mathcal{F}(1)$ is the normalization factor and η_{EW} is a small electroweak correction. In the CLN parameterization we find $\mathcal{F}(1)\eta_{\text{EW}}|V_{cb}| = (35.06 \pm 0.15 \pm 0.56) \times 10^{-3}$, $\rho^2 = 1.106 \pm 0.031 \pm 0.007$, $R_1(1) = 1.229 \pm 0.028 \pm 0.009$, $R_2(1) = 0.852 \pm 0.021 \pm 0.006$. For the BGL parameterization we obtain $\mathcal{F}(1)\eta_{\text{EW}}|V_{cb}| = (34.93 \pm 0.23 \pm 0.59) \times 10^{-3}$, which is consistent with the World Average when correcting for $\mathcal{F}(1)\eta_{\text{EW}}$. The branching fraction of $B^0 \rightarrow D^{*-} \ell^+ \nu_\ell$ is measured to be $\mathcal{B}(B^0 \rightarrow D^{*-} \ell^+ \nu_\ell) = (4.90 \pm 0.02 \pm 0.16)\%$. We also present a new test of lepton flavor universality violation in semileptonic B decays, $\frac{\mathcal{B}(B^0 \rightarrow D^{*-} e^+ \nu_e)}{\mathcal{B}(B^0 \rightarrow D^{*-} \mu^+ \nu_\mu)} = 1.01 \pm 0.01 \pm 0.03$. The errors correspond to the statistical and systematic uncertainties respectively. This is the most precise measurement of $\mathcal{F}(1)\eta_{\text{EW}}|V_{cb}|$ and form factors to date and the first experimental study of the BGL form factor parameterization in an experimental measurement.

I. INTRODUCTION

The decay $B^0 \rightarrow D^{*-} \ell^+ \nu_\ell$ is used to measure the Cabibbo-Kobayashi-Maskawa (CKM) matrix element $|V_{cb}|$ [1, 2], the magnitude of the coupling between b and c quarks in weak interactions, and is a fundamental parameter of the Standard Model (SM). The $B^0 \rightarrow D^{*-} \ell^+ \nu_\ell$ decay is studied in the context of Heavy Quark Effective Theory (HQET) in which the hadronic matrix elements are parameterized by the form factors that can describe this decay. The decay amplitudes of $B^0 \rightarrow D^{*-} \ell^+ \nu_\ell$ are described by three helicity amplitudes which are extracted from the three polarization states of the D^* meson: two transverse polarisation terms, H_\pm , and one longitudinal polarisation term, H_0 .

There exists a long standing tension in the measurement of $|V_{cb}|$ using the inclusive approach, based on the decay mode $B \rightarrow X_c \ell \nu$ and the exclusive approach with $B \rightarrow D^* \ell \nu$. Currently, the world averages for $|V_{cb}|$ for inclusive and exclusive decay modes are [3]:

$$|V_{cb}| = (42.2 \pm 0.8) \times 10^{-3} \text{ (inclusive),} \quad (1)$$

$$|V_{cb}| = (39.1 \pm 0.4) \times 10^{-3} \text{ (CLN, exclusive),} \quad (2)$$

where the errors are the experimental and the theoretical combined. The difference between the inclusive and exclusive approaches is more than 2.5σ . It is thought that the previous theoretical approaches using the CLN form factor parameterization [4] were model dependent and introduced a bias, and therefore model independent form factor approaches based on BGL [5] should be used. In this paper we report data fits with both approaches for the first time. In this paper, the decay is reconstructed in the channel: $B^0 \rightarrow D^{*-} \ell^+ \nu_\ell$ followed by $D^{*-} \rightarrow \bar{D}^0 \pi_s^-$ and $\bar{D}^0 \rightarrow K^- \pi^+$ [6]. This channel offers the best purity for the measurement, which is critical as the measurement will be limited by systematic uncertainties. This is the most precise determination of $|V_{cb}|$ performed with exclusive semileptonic B decays to date. This result supersedes the previous results on $B^0 \rightarrow D^{*-} \ell^+ \nu_\ell$ with an untagged approach from Belle [7]. A major experimental improvement to the efficiency of the track reconstruction

software was implemented in 2011, leading to substantially higher slow pion tracking efficiencies [8] and hence much larger signal yields than in the previous analysis.

II. EXPERIMENTAL APPARATUS AND DATA SAMPLES

We use the full $\Upsilon(4S)$ data sample containing $(772 \pm 11) \times 10^6 B\bar{B}$ pairs equivalent to 711 fb^{-1} of integrated luminosity recorded with the Belle detector [9] at the asymmetric-energy e^+e^- collider KEKB [10]. An additional 88 fb^{-1} of data collected 60 MeV below the $\Upsilon(4S)$ was used for the estimation of $q\bar{q}$ ($q = u, d, s, c$) continuum background.

The Belle detector is a large-solid-angle magnetic spectrometer that consists of a silicon vertex detector (SVD), a 50-layer central drift chamber (CDC), an array of aerogel threshold Cherenkov counters (ACC), a barrel-like arrangement of time-of-flight scintillation counters (TOF), and an electromagnetic calorimeter (ECL) comprised of CsI(Tl) crystals located inside a superconducting solenoid coil that provides a 1.5 T magnetic field. An iron flux-return located outside of the coil is instrumented to detect K_L^0 mesons and to identify muons (KLM). The detector is described in detail elsewhere [9]. Two inner detector configurations were used. A 2.0 cm radius beampipe and a 3-layer silicon vertex detector was used for the first subsample of $152 \times 10^6 B\bar{B}$ pairs (denoted as SVD1), while a 1.5 cm radius beampipe, a 4-layer silicon detector and a small-cell inner drift chamber were used to record the remaining $620 \times 10^6 B\bar{B}$ pairs [11] (denoted as SVD2). We refer to these subsamples later in the paper.

A. Monte Carlo Simulation

Monte Carlo simulated events are used to determine the analysis selection criteria, study the background and estimate the signal reconstruction efficiency. Events with a $B\bar{B}$ pair are generated using EvtGen [12], and the B

meson decays are reproduced based on branching fractions reported in Ref. [13]. The hadronization process of B meson decays that do not have experimentally-measured branching fractions is inclusively reproduced by PYTHIA [14]. For continuum events, the initial quark pair is hadronized by PYTHIA, and hadron decays are modelled by EvtGen. The final-state radiation from charged particles is added using PHOTOS [15]. Detector responses are simulated with GEANT3 [16].

B. Event Reconstruction and Selection Criteria

Charged particle tracks are required to originate from the interaction point, and to have good track fit quality. The criteria for the track impact parameters in the $r - \phi$ and z directions are: $dr < 2$ cm and $|dz| < 4$ cm, respectively. In addition we require that each track has at least one associated hit in any layer of the SVD. For pion and kaon candidates, we use likelihoods determined using the Cherenkov light yield in the ACC, the time-of-flight information from the TOF, and dE/dx from the CDC.

Neutral \bar{D}^0 meson candidates are reconstructed in the clean $\bar{D}^0 \rightarrow K^- \pi^+$ decay channel. The daughter tracks are fitted to a common vertex using a Kalman fit algorithm, with a χ^2 -probability requirement of greater than 10^{-3} to reject misreconstructed \bar{D}^0 candidates. The reconstructed \bar{D}^0 mass is required to be in a window of ± 13.75 MeV/ c^2 from the nominal D^0 mass, corresponding to a width of 2.5σ , determined from data.

The \bar{D}^0 candidates are combined with an additional pion that has a charge opposite that of the kaon, to form D^{*-} candidates. Pions produced in this transition are close to the kinematic threshold, with a mean momentum of approximately 100 MeV/ c , hence are denoted slow pions, π_s^- . There are no SVD hit requirements for slow pions. Another vertex fit is performed between the D^0 and the π_s^- and a χ^2 -probability requirement of greater than 10^{-3} is again imposed. The invariant mass difference between the D^{*-} and the \bar{D}^0 candidates, $\Delta M = M_{D^*} - M_{D^0}$, is first required to be less than 165 MeV/ c^2 for the background fit, and further tightened for the signal yield determination.

Although the contribution from continuum is relatively small in this analysis and it is dominated by charm by fake D^* , we further suppress prompt charm by imposing an upper threshold on the D^* momentum of 2.45 GeV/ c in the center-of-mass (CM) frame (Fig. 1).

Candidate B mesons are reconstructed by combining D^* candidates with an oppositely charged electron or muon. Electron candidates are identified using the ratio of the energy detected in the ECL to the momentum of the track, the ECL shower shape, the distance between the track at the ECL surface and the ECL cluster centre, the energy loss in the CDC (dE/dx) and the response of the ACC. For electron candidates we search for nearby bremsstrahlung photons in a cone of 3 degrees around

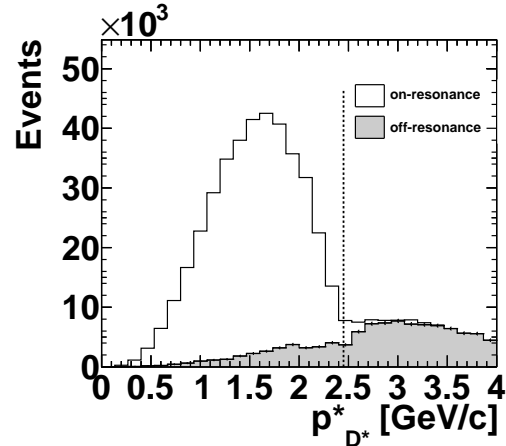


FIG. 1. The D^* momenta in the CM frame, for on-resonance and scaled off-resonance data. The dotted line shows the cut applied for suppression of continuum.

the electron track, and sum the momenta with that of the electron. Muons are identified by their penetration range and transverse scattering in the KLM system. In the momentum region relevant to this analysis, charged leptons are identified with an efficiency of about 90%, while the probabilities to misidentify a pion as an electron and muon are 0.25% and 1.5% respectively [17] [18]. We impose lower thresholds on the momentum of the leptons, such that they reach the respective particle identification detectors for good hadron fake rejection. Here we impose lab frame momentum thresholds of 0.3 GeV/ c for electrons and 0.6 GeV/ c for muons. We furthermore require an upper threshold of 2.4 GeV/ c in the CM frame to reject continuum events.

III. DECAY KINEMATICS

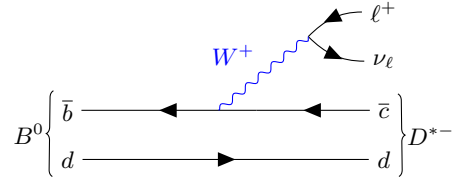


FIG. 2. Tree level Feynman diagram for $B^0 \rightarrow D^{*-} \ell^+ \nu_\ell$.

The tree level transition of the $B^0 \rightarrow D^{*-} \ell^+ \nu_\ell$ decay is shown in Fig. 2. Three angular variables and the hadronic recoil are used to describe this decay. The latter is defined as follows:

$$w = \frac{P_B \cdot P_{D^*}}{m_B m_{D^*}} = \frac{m_B^2 + m_{D^*}^2 - q^2}{2m_B m_{D^*}}, \quad (3)$$

where P_B and P_{D^*} are four momenta of the B and the D^* mesons respectively, m_B, m_{D^*} are their masses, and q^2 is

the invariant mass squared of the lepton-neutrino system. The range of w is restricted by the allowed values of q^2 such that the minimum value of $q_{\min}^2 = m_\ell^2 \approx 0$ GeV 2 corresponds to the maximum value of w ,

$$w_{\max} = \frac{m_B^2 + m_{D^*}^2}{2m_B m_{D^*}}. \quad (4)$$

The three angular variables are depicted in Fig. 3 and are defined as follows:

- θ_ℓ : the angle between the direction of the lepton and the direction opposite the B meson in the virtual W rest frame.
- θ_v : the angle between the direction of the D^0 meson and the direction opposite the B meson in the D^* rest frame.
- χ : the angle between the two planes formed by the decays of the W and the D^* meson, defined in the rest frame of the B^0 meson.

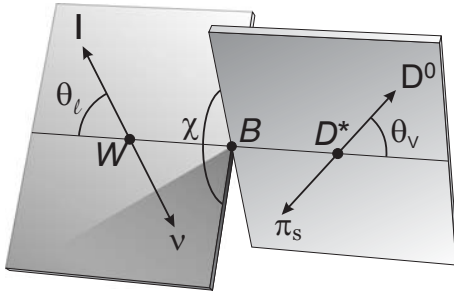


FIG. 3. Definition of the angles θ_ℓ , θ_v and χ for the decay $B^0 \rightarrow D^{*-} \ell^+ \nu_\ell$.

IV. SEMILEPTONIC DECAYS

In the massless lepton limit, the $B^0 \rightarrow D^{*-} \ell^+ \nu_\ell$ differential decay rate is given by [4]

$$\begin{aligned} d\Gamma(B^0 \rightarrow D^{*-} \ell^+ \nu_\ell) &= \\ \frac{dwd \cos \theta_\ell d \cos \theta_v d\chi}{4(4\pi)^2} &= \\ \frac{\eta_{\text{EW}}^2 3m_B m_{D^*}^2 G_F^2 |V_{cb}|^2 \sqrt{w^2 - 1}}{4(4\pi)^2} (1 - 2wr + r^2) & \\ \{(1 - \cos \theta_\ell)^2 \sin^2 \theta_v H_+^2(w) + (1 + \cos \theta_\ell)^2 \sin^2 \theta_v H_-^2(w) & \\ + 4 \sin^2 \theta_\ell \cos^2 \theta_v H_0^2 - 2 \sin^2 \theta_\ell \sin^2 \theta_v \cos 2\chi H_+(w) H_-(w) & \\ - 4 \sin \theta_\ell (1 - \cos \theta_\ell) \sin \theta_v \cos \theta_v \cos \chi H_+(w) H_0(w) & \\ + 4 \sin \theta_\ell (1 + \cos \theta_\ell) \sin \theta_v \cos \theta_v \cos \chi H_-(w) - H_0(w)\} & \end{aligned} \quad (5)$$

where $r = m_{D^*}/m_B$, $G_F = (1.6637 \pm 0.00001) \times 10^{-5} \hbar c^2 \text{GeV}^{-2}$ and η_{EW} is a small electroweak correction (Calculated to be 1.006 in Ref. [19]).

A. The CLN Parameterization

The helicity amplitudes $H_{\pm,0}(w)$ in Eq. 5 are given in terms of three form factors. In the CLN parameterization [4] one writes these helicity amplitudes in terms of the form factor $h_{A_1}(w)$ and the form factor ratios $R_{1,2}(w)$. They are defined as

$$\begin{aligned} h_{A_1}(w) &= h_{A_1}(1) [1 - 8\rho^2 z + (53\rho^2 - 15)z^2 \\ &\quad - (231\rho^2 - 91)z^3], \\ R_1(w) &= R_1(1) - 0.12(w-1) + 0.05(w-1)^2, \\ R_2(w) &= R_2(1) - 0.11(w-1) - 0.06(w-1)^2, \end{aligned} \quad (6)$$

where $z = (\sqrt{w+1} - \sqrt{2})/(\sqrt{w+1} + \sqrt{2})$. In addition to the form factor normalization, there are three independent parameters ρ^2 , $R_1(1)$ and $R_2(1)$. The values of these parameters are not calculated theoretically instead they are extracted by an analysis of experimental data.

B. The BGL Parameterization

A more general parameterization comes from BGL [5], recently used in Refs. [20, 21]. In their approach, the helicity amplitudes H_i are given by

$$\begin{aligned} H_0(w) &= \mathcal{F}_1(w)/\sqrt{q^2}, \\ H_{\pm}(w) &= f(w) \mp m_B m_{D^*} \sqrt{w^2 - 1} g(w). \end{aligned} \quad (7)$$

The three BGL form factors can be written as a series in powers of z ,

$$\begin{aligned} f(z) &= \frac{1}{P_{1+}(z)\phi_f(z)} \sum_{n=0}^{\infty} a_n^f z^n, \\ \mathcal{F}_1(z) &= \frac{1}{P_{1+}(z)\phi_{\mathcal{F}_1}(z)} \sum_{n=0}^{\infty} a_n^{\mathcal{F}_1} z^n, \\ g(z) &= \frac{1}{P_{1-}(z)\phi_g(z)} \sum_{n=0}^{\infty} a_n^g z^n. \end{aligned} \quad (8)$$

In these equations the Blaschke factors, $P_{1\pm}$, are given by

$$P_{1\pm}(z) = \prod_{P=1}^n \frac{z - z_P}{1 - zz_P}, \quad (9)$$

where z_P is defined as

$$z_P = \frac{\sqrt{t_+ - m_P^2} - \sqrt{t_+ - t_-}}{\sqrt{t_+ - m_P^2} + \sqrt{t_+ - t_-}}, \quad (10)$$

while $t_{\pm} = (m_B \pm m_{D^*})^2$ and m_P denotes the masses of the B_c^* resonances. The product is extended to include all the B_c resonances below the $B - D^*$ threshold of 7.29 GeV/c 2 with the appropriate quantum numbers (1^+ for $f(w)$ and $\mathcal{F}_1(w)$, and 1^- for $g(w)$). We use the the B_c resonances listed in Table I. The B_c resonances also enter

TABLE I. The $B_c^{(*)}$ masses used in the Blaschke factors of the BGL parameterization.

Type	Mass (GeV/ c^2)
1^-	6.337
1^-	6.899
1^-	7.012
1^-	7.280
1^+	6.730
1^+	6.736
1^+	7.135
1^+	7.142

the 1^- unitarity bounds as single particle contributions. The outer functions ϕ_i for $i = g, f, \mathcal{F}_1$ are as follows:

$$\begin{aligned} \phi_g(z) &= \sqrt{\frac{n_I}{3\pi\chi_{1-}^T(0)}} \\ &\times \frac{2^4 r^2 (1+z)^2 (1-z)^{-1/2}}{[(1+r)(1-z) + 2\sqrt{r}(1+z)]^4}, \\ \phi_f(z) &= \frac{4r}{m_B^2} \sqrt{\frac{n_I}{3\pi\chi_{1+}^T(0)}} \\ &\times \frac{(1+z)(1-z)^{3/2}}{[(1+r)(1-z) + 2\sqrt{r}(1+z)]^4}, \\ \phi_{\mathcal{F}_1}(z) &= \frac{4r}{m_B^3} \sqrt{\frac{n_I}{6\pi\chi_{1+}^T(0)}} \\ &\times \frac{(1+z)(1-z)^{5/2}}{[(1+r)(1-z) + 2\sqrt{r}(1+z)]^5}, \end{aligned} \quad (11)$$

where $\chi_{1+}^T(0)$ and $\chi_{1-}^T(0)$ are constants given in Table II, and $n_I = 2.6$ represents the number of spectator quarks (three), decreased by a large and conservative SU(3) breaking factor. At zero recoil ($w = 1$ or $z = 0$) there is

TABLE II. Inputs used in the BGL fit.

Input	Value
m_{B^0}	5.279 GeV/ c^2
$m_{D^{*+}}$	2.010 GeV/ c^2
η_{EW}	1.0066
$\chi_{1+}^T(0)$	5.28×10^{-4} (GeV/ c^2) $^{-2}$
$\chi_{1-}^T(0)$	3.07×10^{-4} (GeV/ c^2) $^{-2}$

a relation between two of the form factors,

$$\mathcal{F}_1(0) = (m_B - m_{D^*})f(0). \quad (12)$$

The coefficients of the expansions in Eq. 8 are subject to unitarity bounds based on analyticity and the operator product expansion applied to correlators of two hadronic

$\bar{c}b$ currents:

$$\sum_{i=0}^{\infty} (a_n^g)^2 < 1, \quad \sum_{i=0}^{\infty} [(a_n^f)^2 + (a_n^{\mathcal{F}_1})^2] < 1. \quad (13)$$

They ensure rapid convergence of the z expansion over the whole physical region, $0 < z < 0.056$. The series must be truncated at some power n_{\max} .

V. BACKGROUND ESTIMATION

The most powerful discriminator against background is the cosine of the angle between the B and the $D^*\ell$ momentum vectors in the CM frame under the assumption that the B decays to $D^*\ell\nu$. In the CM frame, the B direction lies on a cone around the $D^*\ell$ axis with an opening angle $2\cos\theta_{B,D^*\ell}$, defined as:

$$\cos\theta_{B,D^*\ell} = \frac{2E_B^* E_{D^*\ell}^* - m_B^2 - m_{D^*\ell}^2}{2|\vec{p}_B^*||\vec{p}_{D^*\ell}^*|}, \quad (14)$$

where E_B^* is half of the CM energy and $|\vec{p}_B^*|$ is $\sqrt{E_B^{*2} - m_B^2}$. The quantities $E_{D^*\ell}^*$, $\vec{p}_{D^*\ell}^*$ and $m_{D^*\ell}$ are determined from the reconstructed $D^*\ell$ system.

The remaining background in the sample is split into the following categories.

- $B \rightarrow D^{**}\ell\nu$, both resonant where D^{**} decays to a D^* , and nonresonant $B \rightarrow D^*\pi\ell\nu$ decays.
- Correlated cascade decays where the D^* and ℓ originate from the same B , e.g. $B \rightarrow D^*\tau\nu$ ($\tau \rightarrow \ell\nu\bar{\nu}$), and $B \rightarrow D^*D$, $D \rightarrow \ell\chi$.
- Uncorrelated decays, where the D^* and ℓ originate from different B mesons in the event.
- Mis-identified leptons (fake leptons): the probability for a hadron being identified as a lepton is small but not negligible in the low momentum region, and is higher for muons.
- Fake D^* candidates, where the D^* is incorrectly reconstructed.
- $q\bar{q}$ continuum, typically $e^+e^- \rightarrow c\bar{c}$.

To model the $B \rightarrow D^{**}\ell\nu$ component, which is comprised of four P -wave resonant modes (D_1 , D_0^* , D_1' , D_2^*) for both neutral and charged B decays, we correct the branching fractions and form factors. The P -wave charm mesons are categorized according to the angular momentum of the light constituent, j_ℓ , namely the $j_\ell^P = 1/2^-$ doublet of D_0^* and D_1' and the $j_\ell^P = 3/2^-$ doublet D_1 and D_2^* . The shapes of the $B \rightarrow D^{**}\ell\nu$ q^2 distributions are corrected to match the predictions of the LLSW model [22]. An additional contribution from nonresonant

modes is considered, although the rate appears to be consistent with zero in recent measurements [23].

To estimate the background yields we perform a binned maximum log likelihood fit of the $D^*\ell$ candidates in three variables, ΔM , $\cos \theta_{B,D^*\ell}$, and p_ℓ . The bin ranges are as follows:

- ΔM : 5 equidistant bins in the range [0.141, 0.156] GeV/c^2 .
- $\cos \theta_{B,D^*\ell}$: 15 equidistant bins in the range [-10, 5].
- p_ℓ : 2 bins in the ranges [0.6, 0.85, 3.0] GeV/c for muons and [0.3, 0.80, 3.0] GeV/c for electrons.

Prior to the fit, the residual continuum background is estimated from off-resonance data and scaled by the off-on resonance integrated luminosities and the $1/s$ dependence of the $e^+e^- \rightarrow q\bar{q}$ cross section. The kinematics of the off and on-resonant continuum background is expected to be slightly different and therefore binned correction weights are determined using MC and applied to the scaled off-resonance data. The remaining background components are modelled with MC simulation after correcting for the most recent decay modelling parameters, and for differences in reconstruction efficiencies between data and MC. Corrections are applied to the lepton identification efficiencies, hadron misidentification rates, and slow pion tracking efficiencies. The data/MC ratios for high momentum tracking efficiencies are consistent with unity and are only considered in the systematic uncertainty estimates. The results from the background fits are in Table III and Fig. 4.

After applying all analysis criteria and subtracting background, a total of 90738 and 89082 $B^0 \rightarrow D^{*-} e^+ \nu_e$ and $B^0 \rightarrow D^{*-} \mu^+ \nu_\mu$ signal decays are found respectively.

VI. MEASUREMENT OF DIFFERENTIAL DISTRIBUTIONS

Measurement of the decay kinematics requires good knowledge of the signal B direction to constrain the neutrino momentum 4-vector. To determine the B direction we estimate the CM frame momentum vector of the non-signal B meson by summing the momenta of the remaining particles in the event ($\vec{p}_{\text{incl.}}^*$) and choose the direction on the cone that minimises the difference to $-p_{\text{incl.}}^*$. To determine $p_{\text{incl.}}^*$ we exclude tracks that do not pass near the interaction point. The impact parameter requirements depend on the transverse momentum of the track, p_T , and are set to:

- $p_T < 250 \text{ MeV}/c$: $dr < 20 \text{ cm}$, $|dz| < 100 \text{ cm}$,
- $p_T < 500 \text{ MeV}/c$: $dr < 15 \text{ cm}$, $|dz| < 50 \text{ cm}$,
- $p_T \geq 500 \text{ MeV}/c$: $dr < 10 \text{ cm}$, $|dz| < 20 \text{ cm}$.

Some track candidates may be counted multiple times, due to low momentum particles spiralling in the CDC, or due to fake tracks fit to a similar set of detector hits as the real track. These are removed by looking for pairs of tracks with similar kinematics, travelling in the same direction with the same electric charge, or in the opposite direction with the opposite electric charge. Isolated clusters that are not matched to the signal particles (i.e. from photons or π^0 decays) are required to have lower energy thresholds to mitigate beam induced background, and are 50, 100 and 150 MeV in the barrel, forward and backward end-cap regions, respectively. We compute $\vec{p}_{\text{incl.}}$ by summing the 3-momenta of the selected particles:

$$\vec{p}_{\text{incl.}} = \sum_i \vec{p}_i , \quad (15)$$

where the index i denotes all isolated clusters and tracks that pass the above criteria. This vector is then translated into the CM frame. The energy component, $E_{\text{incl.}}^*$, is set to the experiment dependent beam energies through $E_{\text{beam}}^* = \sqrt{s}/2$.

We find that the resolutions of the kinematic variables are 0.020 for w , 0.038 for $\cos \theta_\ell$, 0.044 for $\cos \theta_v$ and 0.210 for χ . Based on these resolutions, and the available data sample, we split each distribution into 10 equidistant bins for the $|V_{cb}|$ and form factor fits.

A. Fit to the CLN Parameterization

We perform a binned χ^2 fit to determine the following quantities in the CLN parameterization: the product $\mathcal{F}_1 |V_{cb}|$, and the three parameters ρ^2 , $R_1(1)$ and $R_2(1)$ that parameterise the form factors. We use a set of one-dimensional projections of w , $\cos \theta_\ell$, $\cos \theta_v$ and χ . This reduces complications in the description of the six background components and their correlations across four dimensions. This approach introduces finite bin-to-bin correlations that must be accounted for in the χ^2 calculation.

We choose equidistant binning in each kinematic observable, as described above, and set the ranges according to their kinematically allowed limits. The exception is w : while the kinematically allowed range is between 1 and 1.504, we restrict this to between 1 and 1.50 such that we can ignore the finite mass of the lepton in the interaction.

The number of expected signal events produced in a given bin i , $N_i^{\text{prod.}}$, is given by

$$N_i^{\text{prod.}} = N_{B^0} \mathcal{B}(D^{*+} \rightarrow D^0 \pi^+) \times \mathcal{B}(D^0 \rightarrow K^- \pi^+) \tau_{B^0} \Gamma_i , \quad (16)$$

where N_{B^0} is the number of B^0 mesons in the data sample, $\mathcal{B}(D^{*+} \rightarrow D^0 \pi^+)$ and $\mathcal{B}(D^0 \rightarrow K^- \pi^+)$ are the D^* and D^0 branching ratios into the final state studied in this analysis, τ_{B^0} is the B^0 lifetime, and Γ_i is the width obtained by integrating the CLN theoretical expectation within the corresponding bin boundaries. The values of the D^* and the D^0 branching fractions as well as the B^0

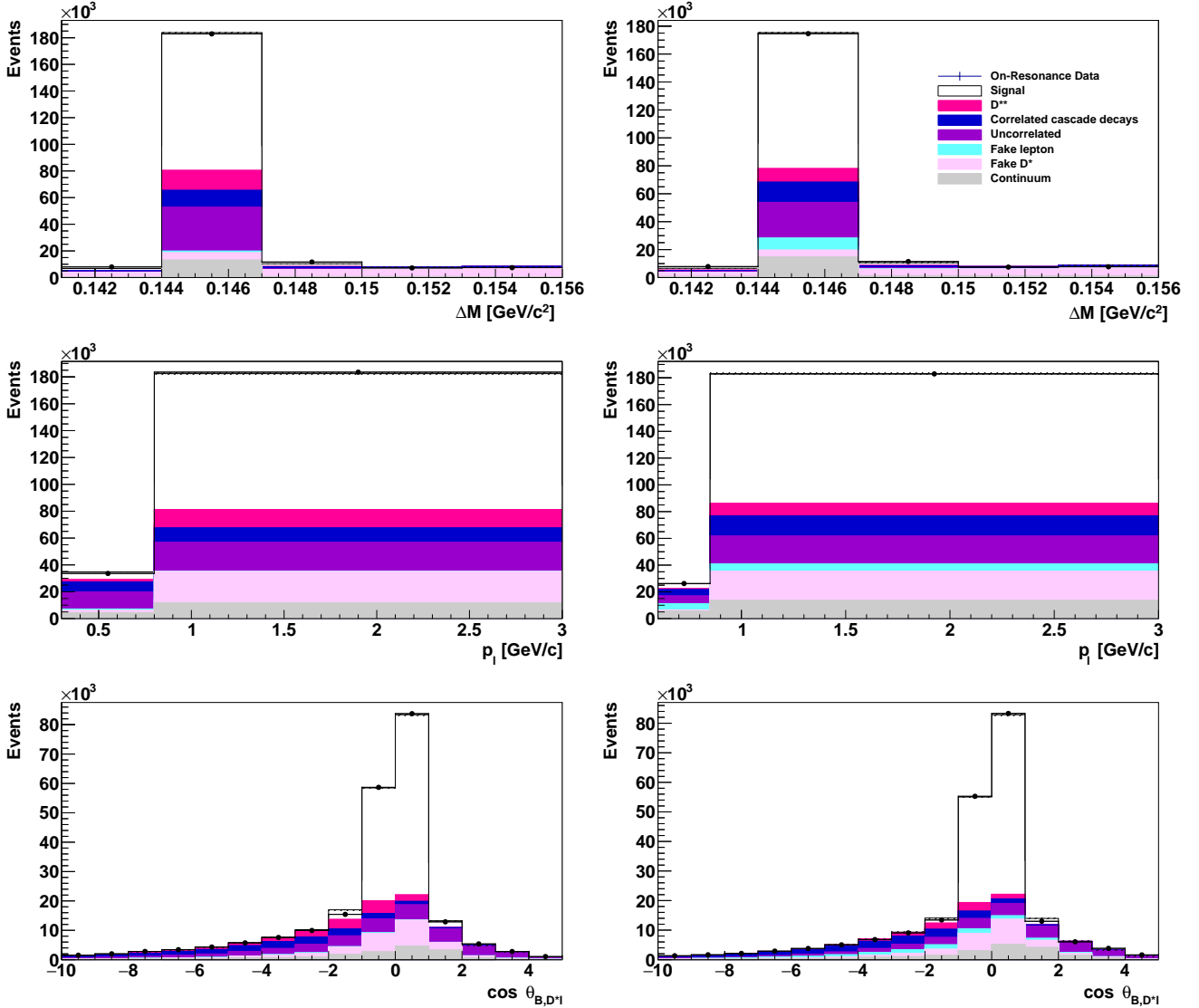


FIG. 4. Result of the fits to the $(\cos \theta_{B,D^*\ell}, \Delta M, p_\ell)$ distributions in the e mode (left) and μ mode (right). The bin boundaries are discussed in the text. The points are on-resonance data, where the uncertainties are smaller than the markers. The colour scheme is defined in the figure.

lifetime are taken from the PDG. The value of N_{B^0} is calculated using $N_{B^0} = 2 \times f_{00} \times N_{BB}$ where N_{BB} is stated in Section II and $f_{00} = 0.486 \pm 0.006$ [3]. The expected number of events, N_i^{exp} , must take into account finite detector resolution and efficiency,

$$N_i^{\text{exp}} = \sum_{j=1}^{40} (R_{ij} \epsilon_j N_j^{\text{prod}}) + N_i^{\text{bkg}}, \quad (17)$$

where ϵ_j is the probability that an event generated in bin j is reconstructed and passes the analysis selection criteria, and R_{ij} is the detector response matrix (the probability that an event generated in bin j is observed in bin i). N_i^{bkg} is the number of expected background events as constrained from the total background yield fit.

In the nominal fit we use the following χ^2 function

based on a forward folding approach:

$$\chi^2 = \sum_{i,j} (N_i^{\text{obs}} - N_i^{\text{exp}}) C_{ij}^{-1} (N_j^{\text{obs}} - N_j^{\text{exp}}), \quad (18)$$

where N_i^{obs} are the number of events observed in bin i of our data sample, and C_{ij}^{-1} is the inverse of the covariance matrix C . The covariance matrix is the variance-covariance matrix whose diagonal elements are the variances and the off-diagonal elements are the covariance of the elements from the i^{th} and j^{th} positions. The covariance is calculated for each pair of bins in either w , $\cos \theta_\ell$, $\cos \theta_V$ and χ . The off-diagonal elements are calculated as,

$$C_{ij} = N \mathcal{P}_{ij} - N \mathcal{P}_i \mathcal{P}_j, \quad \forall i \neq j, \quad (19)$$

TABLE III. Signal and background fractions (%) for events selected in the signal region of ($|\cos \theta_{B,D^* \ell}| < 1$, $0.144 \text{ GeV}/c^2 < \Delta M < 0.147 \text{ GeV}/c^2$, $p_e > 0.80 \text{ GeV}/c$, $p_\mu > 0.85 \text{ GeV}/c$).

	SVD1(e)	SVD1(μ)	SVD2 (e)	SVD2 (μ)
Signal yield	19318	19748	88622	87060
Signal	79.89 ± 0.58	80.12 ± 0.52	81.00 ± 0.19	79.86 ± 0.20
Fake ℓ	0.09 ± 0.16	1.55 ± 0.69	0.10 ± 0.79	1.15 ± 0.38
Fake D^*	3.05 ± 0.09	2.89 ± 0.06	2.94 ± 0.01	2.81 ± 0.01
D^{**}	5.82 ± 0.40	4.00 ± 0.24	5.08 ± 0.14	3.62 ± 0.08
Signal corr.	1.24 ± 0.34	1.99 ± 0.38	1.42 ± 0.07	2.39 ± 0.14
Uncorrelated	5.81 ± 0.50	5.01 ± 0.58	4.96 ± 0.15	5.00 ± 0.24
Continuum	4.11 ± 0.64	4.44 ± 0.74	4.48 ± 0.38	5.16 ± 0.46

where \mathcal{P}_{ij} is the relative probability of the two-dimensional histograms between observable pairs, \mathcal{P}_i and \mathcal{P}_j are the relative probabilities of the one-dimensional histograms of each observable, and N is the total size of the sample. The diagonal elements are the variances of N_i^{exp} and are calculated as,

$$\sigma_i^2 = \sum_{j=1}^{40} \left[R_{ij}^2 \epsilon_j^2 N_j^{\text{th}} + R_{ij}^2 \frac{1-\epsilon_j}{N_{\text{data}}} (N_j^{\text{th}})^2 \right. \\ \left. + R_{ij} \frac{1-R_{ij}}{N'_{\text{data}}} \epsilon_j^2 (N^{\text{th}})^2 + R_{ij}^2 \frac{1-\epsilon_j}{N_{\text{MC}}} \right. \\ \left. + R_{ij} \frac{1-R_{ij}}{N'_{\text{MC}}} \epsilon_j^2 (N_j^{\text{th}})^2 \right] + \sigma^2(N_i^{\text{bkg}}). \quad (20)$$

which uses the Poisson uncertainty associated with the number of events in the MC and data in each bin, and the final term is the total error associated with the background arising from the background fit procedure. We have tested this fit procedure using MC simulated data samples and all results are consistent with expectations, showing no signs of bias. The results from the fit are summarized in Table IV and the fit correlation coefficients are given in Table V. The comparison between data and the form factor fit is shown in Fig. 5.

B. Branching Fraction Measurement

The branching fraction for $\mathcal{B}(B^0 \rightarrow D^{*-} \ell^+ \nu_\ell)$ is obtained with the relation,

$$\mathcal{B} = \frac{N_{\text{signals}}}{\epsilon \times \mathcal{B}(D^{*+} \rightarrow D^0 \pi^+) \times \mathcal{B}(D^0 \rightarrow K^- \pi^+)}, \quad (21)$$

where N_{signals} are signals after applying all the selection criteria, ϵ is the efficiency of the decay, while the values of the branching fractions $\mathcal{B}(D^{*+} \rightarrow D^0 \pi^+)$ and $\mathcal{B}(D^0 \rightarrow K^- \pi^+)$ are taken from PDG. The branching fraction is calculated for all the samples separately, as well as combined.

C. Fit to the BGL Parameterization

To perform the fit to the BGL parameterization we follow the approach in Ref. [20]. We truncate the series in the expansion for a^f and a^g terms at $\mathcal{O}(z^2)$ and order $\mathcal{O}(z^3)$ for a^{F_1} . Due to very large correlations when introducing a_1^g we remove it from the nominal fit results. This results in five free parameters (one more than in the CLN fit), defined as $\tilde{a}_i^f = |V_{cb}| \eta_{\text{EW}} a_i^f$ where $i = 0, 1$, $\tilde{a}_i^g = |V_{cb}| \eta_{\text{EW}} a_i^g$ where $i = 1$ and $\tilde{a}_i^{F_1} = |V_{cb}| \eta_{\text{EW}} a_i^{F_1}$, where $i = 1, 2$. This number of free parameters can describe the data well, while higher order terms will not be well constrained unless additional information from lattice QCD is introduced. We perform a χ^2 fit to the data with the same procedure as for the CLN fit described above. The resulting value for $|V_{cb}|$ is consistent with that from the CLN parameterization. The fit results are given in Table VI and Fig. 6. The linear statistical correlation coefficients are listed in Table VII. Correlations can be high in this fit approach: only the SVD1+SVD2 combined samples are fitted as the fit does not converge well with the smaller SVD1 data set.

VII. SYSTEMATIC UNCERTAINTIES

To estimate systematic uncertainties on the partial branching fractions, form factor parameters, and $|V_{cb}|$, we consider the following sources: background component normalizations, tracking efficiency, charm branching fractions, $B \rightarrow D^{**} \ell \nu$ branching fractions and form factors, the B^0 lifetime, and the number of B^0 mesons in the data sample. The systematic uncertainties on the branching fraction, $\mathcal{F}(1)|V_{cb}|$ and CLN form factor parameters from the CLN fit are summarised in Table VIII, while the uncertainties on the BGL fit are given in Table IX.

We estimate systematic uncertainties by varying each possible uncertainty source such as the PDF shape and signal reconstruction efficiency with the assumption of a Gaussian error, unless otherwise stated. This is done via sets of pseudoexperiments in which each independent sys-

TABLE IV. Fit results for the four sub-samples in the CLN parameterization where the following parameters are floated: ρ^2 , $R_1(1)$, $R_2(1)$ along with $\mathcal{F}(1)|V_{cb}\eta_{EW}|$. The p -value corresponds to the χ^2/ndf using the statistical errors only.

	SVD1 e	SVD1 μ	SVD2 e	SVD2 μ
ρ^2	1.165 ± 0.099	1.165 ± 0.102	1.087 ± 0.046	1.095 ± 0.051
$R_1(1)$	1.326 ± 0.106	1.336 ± 0.103	1.117 ± 0.040	1.287 ± 0.047
$R_2(1)$	0.767 ± 0.073	0.777 ± 0.074	0.861 ± 0.030	0.884 ± 0.034
$\mathcal{F}(1) V_{cb} \eta_{EW} \times 10^3$	34.66 ± 0.48	35.01 ± 0.50	35.25 ± 0.23	34.98 ± 0.25
χ^2/ndf	35/36	36/36	44/36	43/36
p -value	0.52	0.47	0.17	0.20
$\mathcal{B}(B^0 \rightarrow D^{*-} \ell^+ \nu_\ell) [\%]$	4.89 ± 0.06	4.96 ± 0.06	4.93 ± 0.03	4.86 ± 0.03

TABLE V. Statistical correlation matrix of the fit to the full sample in the CLN parameterization.

	ρ^2	$R_1(1)$	$R_2(1)$	$\mathcal{F}(1) V_{cb} $
ρ^2	+1.000	+0.593	-0.883	+0.655
$R_1(1)$		+1.000	-0.692	-0.062
$R_2(1)$			+1.000	-0.268
$\mathcal{F}(1) V_{cb} $				+1.000

tematic uncertainty parameter is randomly varied using a normal distribution. The entire analysis is repeated for each pseudoexperiment and the spread on each measured observable is taken as the systematic error.

The parameters varied are split into two categories, those that affect the shapes and those that affect only the normalization. We start with the former contributions.

- The tracking efficiency corrections for low momentum tracks vary with track p_T , as do the relative uncertainties. We conservatively treat the uncertainties in each slow pion p_T bin to be fully correlated.
- The lepton identification efficiencies are varied according to their respective uncertainties, which are dominated by contributions that are correlated across all bins in p_{lab} and θ_{lab} . The electron and muon systematic uncertainties are calculated separately as well as a combined.
- The results from the background normalization fit are varied within their fitted uncertainties. We take into account finite correlations between the fit results of each component.
- The uncertainty of the decays $B \rightarrow D^{**} \ell^- \bar{\nu}_\ell$ are twofold: the unknown composition of each D^{**} state and the uncertainty in the form-factor parameters used for the MC sample production. The composition uncertainty is estimated based on uncertainties of the branching fractions: $\pm 6\%$ for $\bar{B} \rightarrow D_1(\rightarrow D^* \pi) \ell \bar{\nu}_\ell$, $\pm 12\%$ for $\bar{B} \rightarrow D_2^*(\rightarrow D^* \pi) \ell \bar{\nu}_\ell$, $\pm 24\%$ for $\bar{B} \rightarrow D'_1(\rightarrow D^* \pi \pi) \ell \bar{\nu}_\ell$ and $\pm 17\%$ for

$\bar{B} \rightarrow D_0^*(\rightarrow D^* \pi) \ell \bar{\nu}_\ell$. If the experimentally-measured branching fractions are not applicable, we vary the branching fractions continuously from 0% to 200% in the MC expectation. We estimate an uncertainty arising from the LLSW model parameters by changing the correction factors within the parameter uncertainties.

- The relative number of $B^0 \bar{B}^0$ meson pairs compared to $B^+ B^-$ pairs collected by Belle has a small uncertainty and affects only the relative composition of cross-feed signal events from B^+ and B^0 decays. The fraction $f_{+-}/f_{00} = \mathcal{B}(\Upsilon(4S) \rightarrow B^+ B^-)/\mathcal{B}(\Upsilon(4S) \rightarrow B^0 \bar{B}^0)$ is varied within its uncertainty [24].
- Charged hadron identification uncertainties are determined with data using D^* tagged charm decays.

The uncertainties that only affect the overall normalization are: the tracking efficiency for high momentum tracks, the branching fraction $\mathcal{B}(D^{*+} \rightarrow D^0 \pi^+)$ and $\mathcal{B}(D^0 \rightarrow K^- \pi^+)$, the total number of $\Upsilon(4S)$ events in the sample, and the B^0 lifetime.

VIII. DIFFERENTIAL DATA

In addition to the fit results, we report all necessary data required to perform fits to any choice of form factor parameterization. Specifically we report the background subtracted differential yields (N_{obs}) with the statistical error and the signal efficiency (ϵ) in Table X. The systematic uncertainties in each measured bin are in Tables XI - XIV, the detector response matrices (R) in Tables XV - XVIII for electrons and XIX - XXII for muons. The statistical uncertainty correlations (ρ^{stat}) between measured bins are in Tables XXIII - XXVI for electrons and XXVII - XXX for muons. The systematic uncertainty correlations (ρ^{sys}) between measured bins are given in Tables XXXI - XXXIV.

The correlations between systematic errors in pairs of bins of $(w, \cos \theta_\ell, \cos \theta_v, \chi)$ are determined using a toy MC approach, described in Section VII. The total covariance, for use in the χ^2 minimisation function (Eq. 18) is

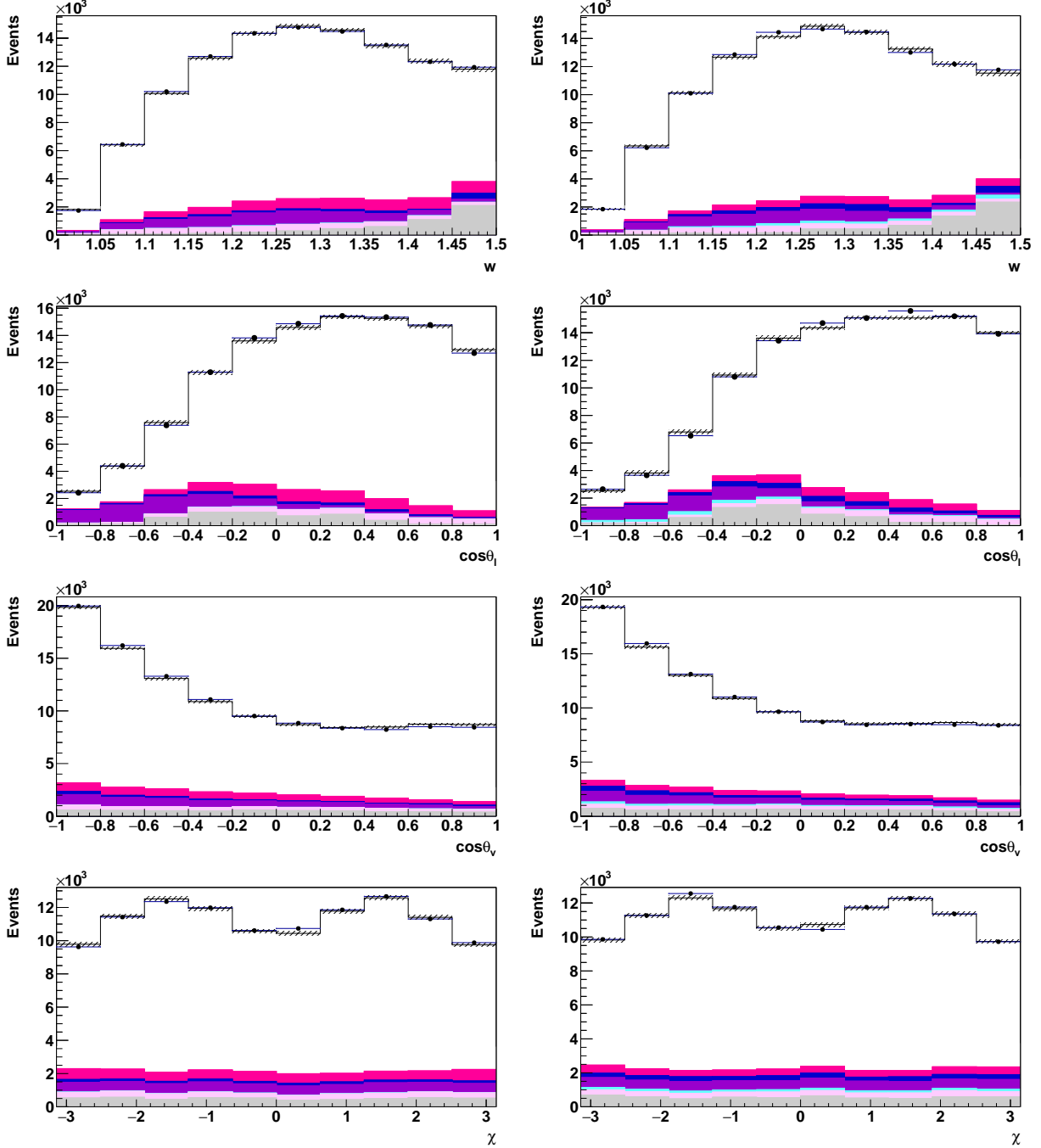


FIG. 5. Results of the fit with the CLN form factor parameterization. The results from the SVD1 and SVD2 samples are added together. The electron modes are on the left and muon modes on the right. The points with error bars are the on-resonance data. Where not shown, the uncertainties are smaller than the black markers. The histograms are, from top to bottom, the signal component, $B \rightarrow D^{**}$ background, signal correlated background, uncorrelated background, fake ℓ component, fake D^* component and continuum.

defined as

$$\text{Cov}_{ij} = \rho_{ij}^{\text{stat}} \sigma_i^{\text{stat}} \sigma_j^{\text{stat}} + \rho_{ij}^{\text{sys}} \sigma_i^{\text{sys}} \sigma_j^{\text{sys}}. \quad (22)$$

As we provide only the background subtracted differen-

tial distributions, the expected yield in Eq. 18 becomes

$$N_i^{\text{exp.}} = \sum_{j=1}^{40} (R_{ij} \epsilon_j N_j^{\text{theory}}). \quad (23)$$

The distributions in w , $\cos \theta_\ell$, $\cos \theta_v$ and χ are divided

TABLE VI. Fit results for the electron and muon sub-samples in the BGL parameterization where the following parameters are floated: \tilde{a}_0^f , \tilde{a}_1^f , $\tilde{a}_1^{F_1}$, $\tilde{a}_2^{F_1}$, \tilde{a}_0^g along with $\mathcal{F}(1)|V_{cb}|\eta_{EW}$ (derived from \tilde{a}_0^f). The p -value corresponds to the χ^2/ndf using the statistical errors only.

	e	μ
$\tilde{a}_0^f \times 10^2$	-0.0507 ± 0.0005	-0.0505 ± 0.0006
$\tilde{a}_1^f \times 10^2$	-0.0673 ± 0.0220	-0.0626 ± 0.0252
$\tilde{a}_1^{F_1} \times 10^2$	-0.0292 ± 0.0086	-0.0247 ± 0.0096
$\tilde{a}_2^{F_1} \times 10^2$	$+0.3407 \pm 0.1674$	$+0.3123 \pm 0.1871$
$\tilde{a}_0^g \times 10^2$	-0.0864 ± 0.0024	-0.0994 ± 0.0027
$\mathcal{F}(1) V_{cb} \eta_{EW} \times 10^3$	35.01 ± 0.31	34.84 ± 0.35
χ^2/ndf	48/35	43/35
p -value	0.08	0.26
$\mathcal{B}(B^0 \rightarrow D^{*-} \ell^+ \nu_\ell) [\%]$	4.91 ± 0.02	4.88 ± 0.03

TABLE VII. Statistical correlation matrix of the fit to the full sample in the BGL parameterization.

	\tilde{a}_0^f	\tilde{a}_1^f	\tilde{a}_1^F	\tilde{a}_2^F	\tilde{a}_0^g
\tilde{a}_0^f	+1.000	-0.790	-0.775	+0.669	-0.038
\tilde{a}_1^f		+1.000	+0.472	-0.411	-0.406
\tilde{a}_1^F			+1.000	-0.981	+0.071
\tilde{a}_2^F				+1.000	-0.057
\tilde{a}_0^g					+1.000

into 10 bins of equal width where the width of each distribution is equal to 0.05, 0.2, 0.2 and $\frac{2\pi}{10}$ respectively. The bins are labelled with a common index i where $i = 1, \dots, 40$. The bins $i = 1, \dots, 10$ correspond to the 10 bins of w distribution with bin ranging from $w = 1.0$ to $w = 1.50$, $i = 11, \dots, 20$ correspond to the 10 bins of $\cos \theta_\ell$ distribution with bin ranging from $\cos \theta_\ell = -1.0$ to $\cos \theta_\ell = +1.0$, $i = 21, \dots, 30$ correspond to the 10 bins of $\cos \theta_v$ distribution with bin ranging from $\cos \theta_v = -1.0$ to $\cos \theta_v = +1.0$ and $i = 31, \dots, 40$ correspond to the 10 bins of χ distribution with the bin ranging from $\chi = -\pi$ to $\chi = \pi$.

The values of $|V_{cb}|$ and the form factors extracted from fits to these data are found to be compatible with the nominal analysis approach used in this paper. The overall uncertainties may be slightly larger as non-linear correlations of systematic uncertainties are not captured by the covariance matrices.

IX. RESULTS

The full results for the CLN fit are given below, where the first uncertainty is statistical, and the second system-

atic:

$$\rho^2 = 1.106 \pm 0.031 \pm 0.007, \quad (24)$$

$$R_1(1) = 1.229 \pm 0.028 \pm 0.009, \quad (25)$$

$$R_2(1) = 0.852 \pm 0.021 \pm 0.006, \quad (26)$$

$$\mathcal{F}(1)|V_{cb}|\eta_{EW} \times 10^3 = 35.06 \pm 0.15 \pm 0.56, \quad (27)$$

$$\mathcal{B}(B^0 \rightarrow D^{*-} \ell^+ \nu_\ell) = (4.90 \pm 0.02 \pm 0.16)\%, \quad (28)$$

where the first error is statistical and the second error is systematic. The dominant systematic uncertainties are the track reconstruction or the lepton ID uncertainty which are correlated between different bins. These results are consistent with, and more precise than, those published in Refs. [7, 25–27]. We find the value of branching fraction is insensitive to the choice of parameterization. We also present the results from the BGL fit, where the first uncertainty is statistical, and the second systematic.

$$\tilde{a}_0^f \times 10^3 = -0.506 \pm 0.004 \pm 0.008, \quad (29)$$

$$\tilde{a}_1^f \times 10^3 = -0.65 \pm 0.17 \pm 0.09, \quad (30)$$

$$\tilde{a}_1^{F_1} \times 10^3 = -0.270 \pm 0.064 \pm 0.023, \quad (31)$$

$$\tilde{a}_2^{F_1} \times 10^3 = +3.27 \pm 1.25 \pm 0.45, \quad (32)$$

$$\tilde{a}_0^g \times 10^3 = -0.929 \pm 0.018 \pm 0.013, \quad (33)$$

$$\mathcal{F}(1)|V_{cb}|\eta_{EW} \times 10^3 = 34.93 \pm 0.23 \pm 0.59, \quad (34)$$

$$\mathcal{B}(B^0 \rightarrow D^{*-} \ell^+ \nu_\ell) = (4.90 \pm 0.02 \pm 0.16)\%. \quad (35)$$

These results are lower than those based on a preliminary tagged approach by Belle [28], as performed in Refs. [20, 21]. Both sets of fits give acceptable χ^2/ndf : therefore the data do not discriminate between the parameterizations. The result with the BGL parameterisation is consistent with the CLN result but has a larger fit uncertainty.

Taking the value of $\mathcal{F}(1) = 0.906 \pm 0.013$ from Lattice QCD in Ref. [29] and $\eta_{EW} = 1.0066$ from Ref. [19], we find the following values for $|V_{cb}|$: $(38.4 \pm 0.2 \pm 0.6 \pm 0.6) \times 10^{-3}$ (CLN+LQCD) and $(38.3 \pm 0.3 \pm 0.7 \pm 0.6) \times 10^{-3}$ (BGL+LQCD). The errors correspond to the statistical, systematic and lattice QCD uncertainties respectively.

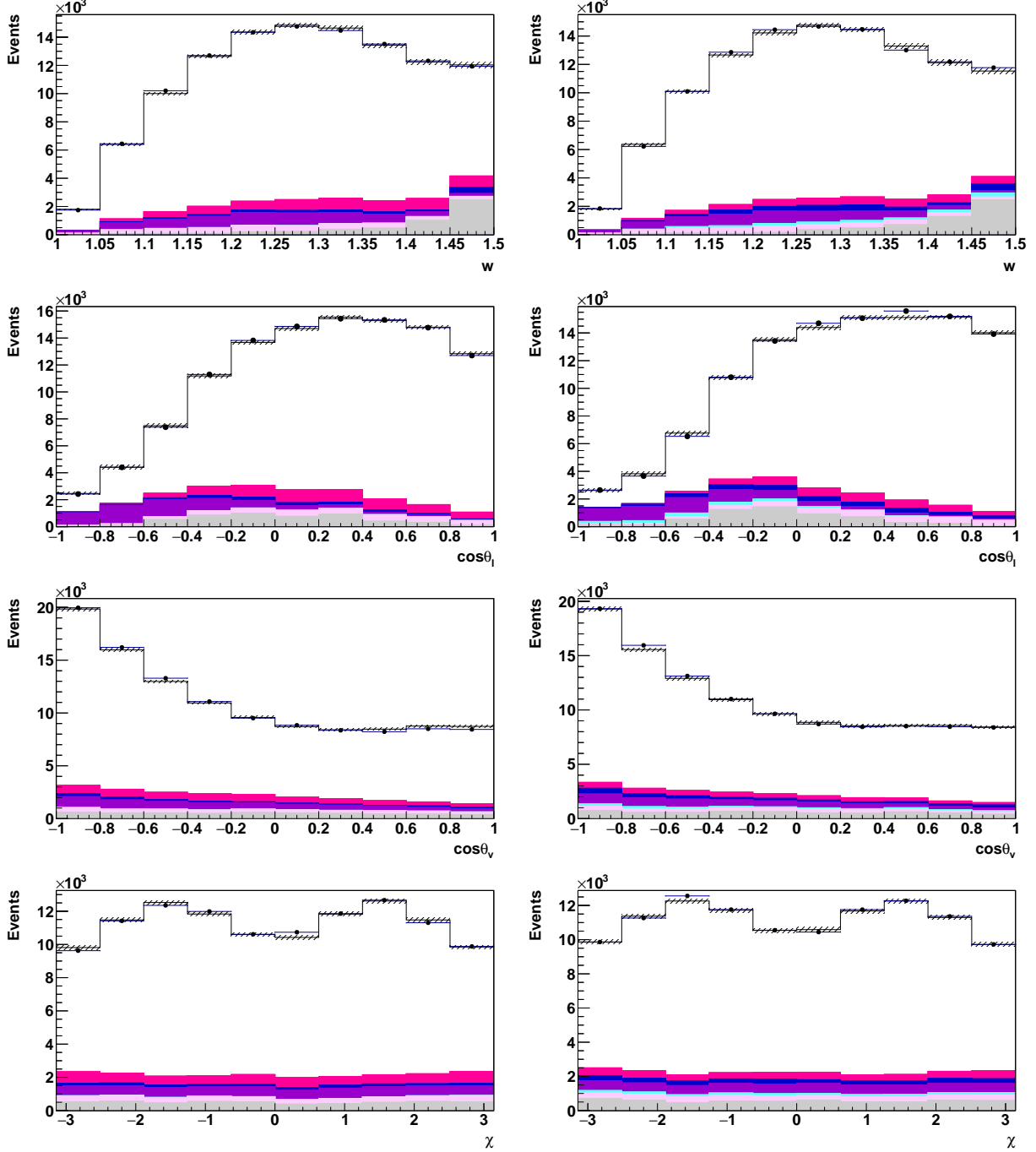


FIG. 6. Results of the fit with the BGL form factor parameterization. The results from the SVD1 and SVD2 samples are added together. The electron modes are on the left and muon modes on the right. The points with error bars are the on-resonance data. Where not shown, the uncertainties are smaller than the black markers. The histograms are, top to bottom, the signal component, $B \rightarrow D^{**}$ background, signal correlated background, uncorrelated background, fake ℓ component, fake D^* component and continuum.

The value of $|V_{cb}|$ from the CLN and BGL parameterizations are consistent with the world average and remain to be in tension with inclusive $|V_{cb}|$ value shown in Eq. 2 and Eq. 1 respectively.

We perform a lepton flavor universality (LFU) test by

forming a ratio of the branching fractions of modes with electrons and muons. The corresponding value of this ratio is

$$\frac{\mathcal{B}(B^0 \rightarrow D^{*-} e^+ \nu)}{\mathcal{B}(B^0 \rightarrow D^{*-} \mu^+ \nu)} = 1.01 \pm 0.01 \pm 0.03 , \quad (36)$$

TABLE VIII. Systematic uncertainty breakdown for $\mathcal{F}(1)|V_{cb}|$, branching fraction and form factor parameters in the CLN parameterization.

Source	ρ^2	$R_1(1)$	$R_2(1)$	$\mathcal{F}(1) V_{cb} $ [%]	$\mathcal{B}(B^0 \rightarrow D^{*-} \ell^+ \nu_\ell)$ [%]
Slow pion efficiency	0.005	0.002	0.001	0.65	1.29
Lepton ID combined	0.001	0.006	0.004	0.68	1.38
$\mathcal{B}(B \rightarrow D^{**} \ell \nu)$	0.002	0.001	0.002	0.26	0.52
$B \rightarrow D^{**} \ell \nu$ form factors	0.003	0.001	0.004	0.11	0.22
f_{+-}/f_{00}	0.001	0.002	0.002	0.52	1.06
Fake e/μ	0.004	0.006	0.001	0.11	0.21
Continuum norm.	0.002	0.002	0.001	0.03	0.06
K/ π ID	< 0.001	< 0.001	< 0.001	0.39	0.77
Fast track efficiency	-	-	-	0.53	1.05
$N\Upsilon(4S)$	-	-	-	0.68	1.37
B^0 lifetime	-	-	-	0.13	0.26
$\mathcal{B}(D^{*+} \rightarrow D^0 \pi_s^+)$	-	-	-	0.37	0.74
$\mathcal{B}(D^0 \rightarrow K\pi)$	-	-	-	0.51	1.02
Total systematic error	0.008	0.009	0.007	1.60	3.21

where the first error is statistical and the second is systematic. The systematic uncertainty is dominated by the electron and muon identification uncertainties, as all others cancel in the ratio. This is the most stringent test of LFU in B decays to date. This result is consistent with unity.

X. CONCLUSION

In this paper we present a new study by the Belle experiment of $B^0 \rightarrow D^{*-} \ell^+ \nu_\ell$ decay. We present the most precise measurement of $|V_{cb}|$ from exclusive decays, and the first direct measurement using the BGL parameterization. The BGL parameterization gives a value for $|V_{cb}|$ consistent with the CLN parameterization, hence the tension remain with the value from inclusive approach [3, 30–32]. We also place stringent bounds on lepton flavor universality, as the semi-electronic and semi-muonic branching fractions have been observed to consistent with each other.

ACKNOWLEDGMENTS

We thank the KEKB group for the excellent operation of the accelerator; the KEK cryogenics group for the efficient operation of the solenoid; and the KEK computer group, and the Pacific Northwest National Laboratory (PNNL) Environmental Molecular Sciences Laboratory (EMSL) computing group for strong computing support;

and the National Institute of Informatics, and Science Information NETwork 5 (SINET5) for valuable network support. We acknowledge support from the Ministry of Education, Culture, Sports, Science, and Technology (MEXT) of Japan, the Japan Society for the Promotion of Science (JSPS), and the Tau-Lepton Physics Research Center of Nagoya University; the Australian Research Council including grants DP180102629, DP170102389, DP170102204, DP150103061, FT130100303; Austrian Science Fund (FWF); the National Natural Science Foundation of China under Contracts No. 11435013, No. 11475187, No. 11521505, No. 11575017, No. 11675166, No. 11705209; Key Research Program of Frontier Sciences, Chinese Academy of Sciences (CAS), Grant No. QYZDJ-SSW-SLH011; the CAS Center for Excellence in Particle Physics (CCEPP); the Shanghai Pujiang Program under Grant No. 18PJ1401000; the Ministry of Education, Youth and Sports of the Czech Republic under Contract No. LTT17020; the Carl Zeiss Foundation, the Deutsche Forschungsgemeinschaft, the Excellence Cluster Universe, and the VolkswagenStiftung; the Department of Science and Technology of India; the Istituto Nazionale di Fisica Nucleare of Italy; National Research Foundation (NRF) of Korea Grants No. 2015H1A2A1033649, No. 2016R1D1A1B01010135, No. 2016K1A3A7A09005603, No. 2016R1D1A1B02012900, No. 2018R1A2B3003643, No. 2018R1A6A1A06024970, No. 2018R1D1A1B07047294; Radiation Science Research Institute, Foreign Large-size Research Facility Application Supporting project, the Global Science Experimental Data

Hub Center of the Korea Institute of Science and Technology Information and KREONET/GLORIAD; the Polish Ministry of Science and Higher Education and the National Science Center; the Grant of the Russian Federation Government, Agreement No. 14.W03.31.0026;

the Slovenian Research Agency; Ikerbasque, Basque Foundation for Science, Spain; the Swiss National Science Foundation; the Ministry of Education and the Ministry of Science and Technology of Taiwan; and the United States Department of Energy and the National Science Foundation.

-
- [1] M. Kobayashi and T. Maskawa, Prog. Theor. Phys. **49**, 652 (1973).
 - [2] N. Cabibbo, Phys. Rev. Lett. **10**, 531 (1963).
 - [3] Y. Amhis *et al.* (HFLAV Group), Eur. Phys. J. C **77**, 895 (2017).
 - [4] I. Caprini, L. Lellouch and M. Neubert, Nucl. Phys. B **530** 153 (1998).
 - [5] C. G. Boyd, B. Grinstein, and R. F. Lebed, Phys. Rev. D **56**, 6895 (1997).
 - [6] Throughout this note charge-conjugate decay modes are implied.
 - [7] W. Dungel *et al.* (Belle Collab.), Phys. Rev. D **82**, 112007 (2010).
 - [8] J. Brodzicka *et al.* (Belle Collab.), PTEP **2012**, 04D001 (2012)
 - [9] A. Abashian *et al.* (Belle Collab.), Nucl. Instr. and Meth. A **479**, 117 (2002).
 - [10] S. Kurokawa and E. Kikutani, Nucl. Instrum. Methods Phys. Res. Sect. A **499**, 1 (2003), and other papers included in this Volume; T. Abe *et al.*, Prog. Theor. Exp. Phys. **2013**, 03A001 (2013) and references therein.
 - [11] Z. Natkaniec *et al.* (Belle SVD2 Group), Nucl. Instr. and Meth. A **560**, 1 (2006).
 - [12] D. J. Lange, Nucl. Instr. and Meth. A **462**, 152 (2001).
 - [13] C. Patrignani *et al.* (Particle Data Group), Chin. Phys. C **40**, 100001 (2016).
 - [14] T. Sjøstrand, S. Mrenna and P. Skands, J. High Energy Phys., **05**, 026 (2006).
 - [15] N. Davidson, T. Przedzinski and Z. Was, Comput. Phys. Commun. **199**, 86 (2016).
 - [16] R. Brun *et al.*, GEANT 3.21, CERN Report DD/EE/84-1, 1984 (unpublished).
 - [17] K. Hanagaki, H. Kakuno, H. Ikeda, T. Iijima and T. Tsukamoto, Nucl. Instrum. Meth. A **485**, 490 (2002).
 - [18] A. Abashian *et al.*, Nucl. Instrum. Meth. A **491**, 69 (2002).
 - [19] A. Sirlin, Nucl. Phys. B **196**, 83 (1982).
 - [20] B. Grinstein and A. Kobach, Phys. Lett. B **771**, 359 (2017).
 - [21] D. Bigi, P. Gambino and S. Schacht, Phys. Lett. B **769**, 441 (2017).
 - [22] A. K. Leibovich, Z. Ligeti, I. W. Stewart and M. B. Wise, Phys. Rev. D **57**, 308 (1998).
 - [23] A. Vossen *et al.* (Belle Collab.), Phys. Rev. D **98**, no. 1, 012005 (2018)
 - [24] K. Nakamura *et al.* [Particle Data Group], J. Phys. G **37**, 075021 (2010).
 - [25] B. Aubert *et al.* (BaBar Collab.) Phys. Rev. D **77**, 032002 (2008).
 - [26] B. Aubert *et al.* (BaBar Collab.), Phys. Rev. Lett. **100**, 231803 (2008).
 - [27] B. Aubert *et al.* (BaBar Collab.), Phys. Rev. D **79**, 012002 (2009).
 - [28] A. Abdesselam *et al.* (Belle Collab.),
 - [29] J. A. Bailey *et al.* (Fermilab Lattice, MILC), Phys. Rev. D **89**, 114504 (2014).
 - [30] P. Urquijo *et al.* (Belle Collab.), Phys. Rev. D **75**, 032001 (2007).
 - [31] C. Schwanda *et al.* (Belle Collab.), Phys. Rev. D **75**, 032005 (2007).
 - [32] A. Alberti, P. Gambino, K. J. Healey and S. Nandi, Phys. Rev. Lett. **114**, 061802 (2015)

TABLE IX. Systematic uncertainty breakdown for $\mathcal{F}(1)|V_{cb}|$, branching fraction and form factor parameters in the BGL parameterization.

Source	\tilde{a}_0^f [%]	\tilde{a}_1^f [%]	\tilde{a}_1^{F1} [%]	\tilde{a}_2^{F1} [%]	\tilde{a}_0^g [%]	$\eta_{EW}\mathcal{F}(1) V_{cb} $ [%]	$\mathcal{B}(B^0 \rightarrow D^{*-} \ell^+ \nu_\ell)$ [%]
Slow pion efficiency	0.79	9.59	5.61	4.46	0.18	0.79	1.57
Lepton ID combined	0.67	5.45	1.35	0.73	0.38	0.67	1.33
$\mathcal{B}(B \rightarrow D^{**} \ell \nu)$	0.05	5.02	4.34	9.31	0.37	0.05	0.10
$B \rightarrow D^{**} \ell \nu$ form factors	0.08	2.08	3.56	6.78	0.12	0.08	0.16
f_{+-}/f_{00}	0.56	0.46	0.50	0.48	0.56	0.56	1.05
Fake e/μ	0.07	6.43	3.03	5.92	0.14	0.07	0.11
K/ π ID	0.39	0.39	0.39	0.39	0.39	0.39	0.77
Fast track efficiency	0.53	0.53	0.53	0.53	0.53	0.53	1.05
$N(\Upsilon(4S))$	0.69	0.69	0.69	0.69	0.69	0.69	1.37
B^0 lifetime	0.13	0.13	0.13	0.13	0.13	0.13	0.26
$\mathcal{B}(D^{*+} \rightarrow D^0 \pi_s^+)$	0.37	0.37	0.37	0.37	0.37	0.37	0.74
$\mathcal{B}(D^0 \rightarrow K\pi)$	0.51	0.51	0.51	0.51	0.51	0.51	1.02
Total systematic error	1.65	13.93	8.69	13.77	1.40	1.65	3.26

TABLE X. Background subtracted signal yield and selection efficiency in the 40 bins defined in Section VIII. The left (right) part of the table is for the electron (muon) mode. Only statistical uncertainty is quoted.

Bin	Yield	Efficiency (%)	Yield	Efficiency (%)
1	1421 ± 41	2.72 ± 0.02	1494 ± 43	2.68 ± 0.02
2	5319 ± 85	5.72 ± 0.02	5062 ± 89	5.66 ± 0.02
3	8563 ± 113	7.70 ± 0.03	8385 ± 120	7.66 ± 0.03
4	10685 ± 129	9.10 ± 0.03	10734 ± 142	9.05 ± 0.03
5	11971 ± 156	10.03 ± 0.03	11961 ± 159	9.91 ± 0.03
6	12275 ± 167	10.61 ± 0.03	12090 ± 167	10.43 ± 0.03
7	11888 ± 166	10.74 ± 0.03	11803 ± 168	10.60 ± 0.03
8	11096 ± 151	10.67 ± 0.03	10501 ± 155	10.52 ± 0.03
9	9751 ± 159	10.23 ± 0.03	9378 ± 160	10.04 ± 0.03
10	7770 ± 215	9.10 ± 0.03	7673 ± 213	9.14 ± 0.03
11	1305 ± 79	3.12 ± 0.03	1240 ± 95	3.16 ± 0.03
12	2650 ± 142	3.97 ± 0.02	1983 ± 110	3.52 ± 0.02
13	4902 ± 154	5.73 ± 0.02	3971 ± 150	5.19 ± 0.02
14	8295 ± 172	7.96 ± 0.03	7365 ± 193	7.59 ± 0.03
15	10748 ± 187	9.31 ± 0.03	9841 ± 213	9.10 ± 0.03
16	12118 ± 182	9.85 ± 0.03	11893 ± 190	9.78 ± 0.03
17	12681 ± 219	10.23 ± 0.03	12646 ± 181	10.27 ± 0.03
18	13282 ± 157	10.59 ± 0.03	13663 ± 149	10.43 ± 0.03
19	13133 ± 152	11.06 ± 0.03	13659 ± 143	11.00 ± 0.03
20	11624 ± 119	11.21 ± 0.03	12820 ± 123	11.36 ± 0.03
21	16815 ± 195	11.72 ± 0.03	15991 ± 205	11.54 ± 0.03
22	13427 ± 180	11.52 ± 0.03	13157 ± 177	11.43 ± 0.03
23	10797 ± 152	11.35 ± 0.03	10533 ± 159	11.14 ± 0.03
24	8706 ± 139	10.88 ± 0.04	8574 ± 147	10.74 ± 0.04
25	7227 ± 133	10.20 ± 0.04	7353 ± 137	10.09 ± 0.04
26	6802 ± 127	9.34 ± 0.04	6599 ± 127	9.29 ± 0.04
27	6477 ± 122	8.29 ± 0.03	6515 ± 122	8.25 ± 0.03
28	6518 ± 123	7.16 ± 0.03	6614 ± 129	7.10 ± 0.03
29	6920 ± 122	6.05 ± 0.02	6832 ± 123	5.97 ± 0.02
30	7050 ± 114	4.82 ± 0.02	6914 ± 119	4.72 ± 0.02
31	7286 ± 142	8.60 ± 0.03	7361 ± 146	8.51 ± 0.03
32	9173 ± 140	8.74 ± 0.03	8923 ± 146	8.67 ± 0.03
33	10279 ± 146	8.96 ± 0.03	10466 ± 146	8.82 ± 0.03
34	9892 ± 143	9.30 ± 0.03	9540 ± 149	9.15 ± 0.03
35	8443 ± 142	9.81 ± 0.03	8319 ± 144	9.70 ± 0.03
36	8745 ± 132	9.82 ± 0.03	8197 ± 140	9.73 ± 0.03
37	9808 ± 144	9.33 ± 0.03	9661 ± 144	9.20 ± 0.03
38	10505 ± 144	9.00 ± 0.03	10162 ± 145	8.83 ± 0.03
39	9089 ± 141	8.77 ± 0.03	9062 ± 148	8.62 ± 0.03
40	7518 ± 137	8.59 ± 0.03	7391 ± 142	8.54 ± 0.03

TABLE XI. Systematic uncertainty (%) in each bin of the observable w . The bins are defined in Section VIII.

Source	1	2	3	4	5	6	7	8	9	10
$\mathcal{B}(D^0 \rightarrow K\pi)$	1.02	1.02	1.02	1.01	1.01	1.02	1.02	1.02	1.02	1.02
$\mathcal{B}(D^{*+} \rightarrow D^0 \pi_s^+)$	0.74	0.74	0.74	0.74	0.74	0.74	0.74	0.74	0.74	0.71
Lepton ID(e)	1.38	1.48	1.58	1.57	1.80	1.89	1.90	2.02	2.04	2.05
Lepton ID(μ)	2.23	2.12	2.05	2.01	2.04	2.05	2.04	2.03	1.93	1.93
Lepton ID	1.18	1.21	1.25	1.24	1.35	1.39	1.39	1.43	1.40	1.41
Slow track efficiency	5.77	3.01	2.14	1.75	1.53	1.38	1.33	1.26	1.12	0.84
e/μ fake rate	0.03	0.01	0.04	0.06	0.12	0.12	0.13	0.17	0.27	0.17
D^{**} branching fraction	0.44	0.15	0.01	0.41	0.06	0.04	0.08	0.60	0.35	0.22
D^{**} shape	0.02	0.11	0.14	0.01	0.16	0.30	0.22	0.08	0.35	0.92
f_{+-}/f_{00}	1.05	1.07	1.10	1.10	1.09	1.08	1.11	1.08	1.05	1.08
Norm. continuum	0.06	0.06	0.06	0.06	0.06	0.06	0.06	0.06	0.06	0.06
Fast track efficiency	1.05	1.05	1.05	1.05	1.05	1.05	1.05	1.05	1.05	1.05
$N(\Upsilon(4S))$	1.37	1.37	1.37	1.37	1.37	1.37	1.37	1.37	1.37	1.37
B^0 lifetime	0.26	0.26	0.26	0.26	0.26	0.26	0.26	0.26	0.26	0.26
K/π ID	0.77	0.77	0.77	0.77	0.77	0.77	0.77	0.77	0.77	0.77
Total	6.42	4.12	3.55	3.35	3.26	3.22	3.20	3.23	3.14	3.16

TABLE XII. Systematic uncertainty (%) in each bin of the observable $\cos \theta_\ell$. The bins are defined in Section VIII.

Source	11	12	13	14	15	16	17	18	19	20
$\mathcal{B}(D^0 \rightarrow K\pi)$	1.02	1.02	1.02	1.03	1.02	1.01	1.02	1.02	1.02	1.02
$\mathcal{B}(D^{*+} \rightarrow D^0 \pi_s^+)$	0.74	0.74	0.74	0.74	0.74	0.74	0.74	0.74	0.74	0.74
Lepton ID(e)	4.26	4.07	3.54	2.66	1.94	1.41	1.43	1.40	1.46	1.52
Lepton ID(μ)	2.52	2.67	2.60	2.18	2.04	2.05	1.93	1.95	1.94	1.74
Lepton ID	2.17	2.23	2.09	1.68	1.41	1.16	1.15	1.14	1.17	1.14
Slow track efficiency	2.83	1.95	1.49	1.28	1.27	1.30	1.33	1.38	1.45	1.52
e/μ fake rate	0.30	0.13	0.05	0.10	0.12	0.14	0.15	0.15	0.11	0.13
D^{**} branching fraction	0.15	0.13	0.11	0.15	0.10	0.05	0.06	0.08	0.05	0.08
D^{**} shape	0.10	0.10	0.15	0.11	0.10	0.14	0.06	0.08	0.02	0.07
f_{+-}/f_{00}	1.08	1.08	1.08	1.07	1.08	1.07	1.09	1.09	1.08	1.05
Norm. continuum	0.06	0.06	0.06	0.06	0.06	0.06	0.06	0.06	0.06	0.06
Fast track efficiency	1.05	1.05	1.05	1.05	1.05	1.05	1.05	1.05	1.05	1.05
$N(\Upsilon(4S))$	1.37	1.37	1.37	1.37	1.37	1.37	1.37	1.37	1.37	1.37
B^0 lifetime	0.26	0.26	0.26	0.26	0.26	0.26	0.26	0.26	0.26	0.26
K/π ID	0.77	0.77	0.77	0.77	0.77	0.77	0.77	0.77	0.77	0.77
Total	4.39	3.90	3.61	3.30	3.17	3.07	3.09	3.10	3.14	3.16

TABLE XIII. Systematic uncertainty (%) in each bin of the observable $\cos \theta_v$. The bins are defined in Section VIII.

Source	21	22	23	24	25	26	27	28	29	30
$\mathcal{B}(D^0 \rightarrow K\pi)$	1.02	1.02	1.02	1.02	1.02	1.02	1.02	1.02	1.02	1.02
$\mathcal{B}(D^{*+} \rightarrow D^0 \pi_s^+)$	0.74	0.74	0.74	0.74	0.74	0.74	0.74	0.74	0.74	0.74
Lepton ID(e)	1.95	1.91	1.83	1.72	1.62	1.65	1.72	1.83	1.90	1.94
Lepton ID(μ)	2.15	2.13	2.09	2.04	2.05	1.90	1.96	1.93	1.90	1.86
Lepton ID	1.44	1.42	1.38	1.31	1.27	1.24	1.29	1.33	1.34	1.34
Slow track efficiency	1.02	1.14	1.28	1.39	1.52	1.68	1.84	1.99	2.18	2.63
e/μ fake rate	0.04	0.06	0.11	0.16	0.22	0.19	0.18	0.17	0.21	0.04
D^{**} branching fraction	0.08	0.01	0.17	0.32	0.27	0.19	0.07	0.14	0.18	0.33
D^{**} shape	0.07	0.03	0.02	0.05	0.16	0.12	0.05	0.19	0.00	0.08
f_{+-}/f_{00}	1.08	1.08	1.07	1.09	1.07	1.09	1.10	1.08	1.10	1.08
Norm. continuum	0.06	0.06	0.06	0.06	0.06	0.06	0.06	0.06	0.06	0.06
Fast track efficiency	1.05	1.05	1.05	1.05	1.05	1.05	1.05	1.05	1.05	1.05
$N(\Upsilon(4S))$	1.37	1.37	1.37	1.37	1.37	1.37	1.37	1.37	1.37	1.37
B^0 lifetime	0.26	0.26	0.26	0.26	0.26	0.26	0.26	0.26	0.26	0.26
K/π ID	0.77	0.77	0.77	0.77	0.77	0.77	0.77	0.77	0.77	0.77
Total	3.09	3.12	3.16	3.19	3.23	3.30	3.39	3.49	3.62	3.90

TABLE XIV. Systematic uncertainty (%) in each bin of the observable χ . The bins are defined in Section VIII.

Source	31	32	33	34	35	36	37	38	39	40
$\mathcal{B}(D^0 \rightarrow K\pi)$	1.02	1.02	1.02	1.02	1.02	1.02	1.02	1.02	1.02	1.02
$\mathcal{B}(D^{*+} \rightarrow D^0 \pi_s^+)$	0.74	0.74	0.74	0.74	0.74	0.74	0.74	0.74	0.74	0.74
Lepton ID(e)	1.81	1.77	1.83	1.80	1.82	1.84	1.85	1.86	1.83	1.82
Lepton ID(μ)	1.89	1.97	2.08	2.06	2.09	2.08	2.12	1.99	1.95	1.87
Lepton ID	1.31	1.32	1.38	1.36	1.37	1.38	1.39	1.36	1.34	1.30
Slow track efficiency	1.47	1.45	1.40	1.33	1.28	1.31	1.36	1.45	1.47	1.46
e/μ fake rate	0.15	0.10	0.09	0.12	0.16	0.11	0.09	0.13	0.13	0.16
D^{**} branching fraction	0.15	0.10	0.01	0.03	0.06	0.02	0.03	0.13	0.02	0.16
D^{**} shape	0.01	0.07	0.01	0.09	0.08	0.07	0.01	0.13	0.13	0.00
f_{+-}/f_{00}	11.08	1.07	1.09	1.06	1.08	1.07	1.09	1.08	1.06	1.10
Norm. continuum	0.06	0.06	0.06	0.06	0.06	0.06	0.06	0.06	0.06	0.06
Fast track efficiency	1.05	1.05	1.05	1.05	1.05	1.05	1.05	1.05	1.05	1.05
$N(\Upsilon(4S))$	1.37	1.37	1.37	1.37	1.37	1.37	1.37	1.37	1.37	1.37
B^0 lifetime	0.26	0.26	0.26	0.26	0.26	0.26	0.26	0.26	0.26	0.26
K/π ID	0.77	0.77	0.77	0.77	0.77	0.77	0.77	0.77	0.77	0.77
Total	3.21	3.20	3.20	3.16	3.16	3.16	3.20	3.22	3.22	3.21

TABLE XV. Response matrix R for observable w for the electron mode. The bins are defined in Section VIII.

Bin	1	2	3	4	5	6	7	8	9	10
1	0.803	0.053	0.000	0.000	0.000	0.000	0.000	0.000	0.000	0.000
2	0.197	0.778	0.098	0.000	0.000	0.000	0.000	0.000	0.000	0.000
3	0.000	0.168	0.717	0.126	0.002	0.000	0.000	0.000	0.000	0.000
4	0.000	0.001	0.182	0.667	0.149	0.006	0.000	0.000	0.000	0.000
5	0.000	0.000	0.004	0.199	0.626	0.167	0.011	0.000	0.000	0.000
6	0.000	0.000	0.000	0.009	0.207	0.592	0.177	0.015	0.000	0.000
7	0.000	0.000	0.000	0.000	0.016	0.215	0.575	0.183	0.018	0.000
8	0.000	0.000	0.000	0.000	0.000	0.021	0.213	0.567	0.186	0.017
9	0.000	0.000	0.000	0.000	0.000	0.000	0.024	0.214	0.598	0.186
10	0.000	0.000	0.000	0.000	0.000	0.000	0.000	0.022	0.198	0.797

TABLE XVI. Response matrix R for observable $\cos \theta_\ell$ for the electron mode. The bins are defined in Section VIII.

Bin	1	2	3	4	5	6	7	8	9	10
1	0.961	0.024	0.000	0.000	0.000	0.000	0.000	0.000	0.000	0.000
2	0.038	0.952	0.027	0.000	0.000	0.000	0.000	0.000	0.000	0.000
3	0.000	0.021	0.948	0.041	0.001	0.000	0.000	0.000	0.000	0.000
4	0.000	0.001	0.023	0.918	0.067	0.003	0.001	0.001	0.001	0.000
5	0.000	0.001	0.001	0.040	0.871	0.097	0.005	0.001	0.001	0.000
6	0.000	0.000	0.000	0.001	0.060	0.817	0.129	0.006	0.001	0.000
7	0.000	0.000	0.000	0.000	0.001	0.082	0.758	0.164	0.007	0.001
8	0.000	0.000	0.000	0.000	0.000	0.001	0.106	0.698	0.196	0.008
9	0.000	0.000	0.000	0.000	0.000	0.000	0.001	0.128	0.657	0.212
10	0.000	0.000	0.000	0.000	0.000	0.000	0.000	0.002	0.137	0.777

TABLE XVII. Response matrix R for observable $\cos \theta_v$ for the electron mode. The bins are defined in Section VIII.

Bin	1	2	3	4	5	6	7	8	9	10
1	0.918	0.077	0.000	0.000	0.000	0.000	0.000	0.000	0.000	0.000
2	0.082	0.806	0.095	0.001	0.000	0.000	0.000	0.000	0.000	0.000
3	0.000	0.115	0.761	0.101	0.002	0.000	0.000	0.000	0.000	0.000
4	0.000	0.001	0.141	0.735	0.105	0.002	0.000	0.000	0.000	0.000
5	0.000	0.000	0.002	0.160	0.719	0.100	0.001	0.000	0.000	0.000
6	0.000	0.000	0.000	0.003	0.170	0.722	0.093	0.001	0.000	0.000
7	0.000	0.000	0.000	0.000	0.003	0.173	0.738	0.080	0.001	0.000
8	0.000	0.000	0.000	0.000	0.000	0.002	0.166	0.771	0.072	0.000
9	0.000	0.000	0.000	0.000	0.000	0.000	0.001	0.147	0.819	0.064
10	0.000	0.000	0.000	0.000	0.000	0.000	0.000	0.001	0.108	0.936

TABLE XVIII. Response matrix R for observable χ for the electron mode. The bins are defined in Section VIII.

Bin	1	2	3	4	5	6	7	8	9	10
1	0.659	0.129	0.011	0.003	0.002	0.002	0.002	0.004	0.013	0.144
2	0.151	0.691	0.132	0.012	0.004	0.002	0.002	0.002	0.004	0.016
3	0.015	0.141	0.697	0.147	0.016	0.005	0.002	0.002	0.002	0.005
4	0.005	0.012	0.134	0.671	0.162	0.018	0.005	0.002	0.002	0.002
5	0.002	0.004	0.013	0.140	0.634	0.155	0.016	0.004	0.002	0.002
6	0.002	0.002	0.004	0.015	0.155	0.633	0.141	0.013	0.004	0.003
7	0.002	0.002	0.002	0.004	0.018	0.163	0.670	0.136	0.012	0.004
8	0.005	0.002	0.002	0.002	0.005	0.015	0.147	0.695	0.140	0.015
9	0.016	0.004	0.002	0.002	0.002	0.004	0.013	0.132	0.691	0.150
10	0.142	0.013	0.003	0.002	0.002	0.002	0.003	0.012	0.130	0.659

TABLE XIX. Response matrix R for observable w for the muon mode. The bins are defined in Section VIII.

Bin	1	2	3	4	5	6	7	8	9	10
1	0.812	0.051	0.000	0.000	0.000	0.000	0.000	0.000	0.000	0.000
2	0.188	0.784	0.096	0.000	0.000	0.000	0.000	0.000	0.000	0.000
3	0.000	0.164	0.728	0.126	0.002	0.000	0.000	0.000	0.000	0.000
4	0.000	0.001	0.172	0.676	0.149	0.006	0.000	0.000	0.000	0.000
5	0.000	0.000	0.004	0.190	0.631	0.165	0.010	0.000	0.000	0.000
6	0.000	0.000	0.000	0.008	0.203	0.600	0.181	0.016	0.000	0.000
7	0.000	0.000	0.000	0.000	0.014	0.209	0.578	0.187	0.019	0.000
8	0.000	0.000	0.000	0.000	0.000	0.020	0.209	0.573	0.195	0.017
9	0.000	0.000	0.000	0.000	0.000	0.000	0.022	0.205	0.600	0.195
10	0.000	0.000	0.000	0.000	0.000	0.000	0.000	0.019	0.186	0.788

TABLE XX. Response matrix R for observable $\cos \theta_\ell$ for the muon mode. The bins are defined in Section VIII.

Bin	1	2	3	4	5	6	7	8	9	10
1	0.959	0.022	0.000	0.000	0.000	0.000	0.000	0.000	0.000	0.000
2	0.039	0.955	0.012	0.000	0.000	0.000	0.000	0.000	0.000	0.000
3	0.000	0.021	0.960	0.022	0.001	0.000	0.000	0.000	0.000	0.000
4	0.001	0.001	0.026	0.931	0.043	0.001	0.000	0.000	0.000	0.000
5	0.000	0.000	0.001	0.047	0.889	0.070	0.002	0.000	0.000	0.000
6	0.000	0.001	0.000	0.000	0.067	0.837	0.103	0.002	0.001	0.000
7	0.000	0.000	0.000	0.000	0.000	0.091	0.778	0.138	0.003	0.000
8	0.000	0.000	0.000	0.000	0.000	0.000	0.117	0.715	0.174	0.004
9	0.000	0.000	0.000	0.000	0.000	0.000	0.001	0.142	0.672	0.193
10	0.000	0.000	0.000	0.000	0.000	0.000	0.000	0.002	0.151	0.803

TABLE XXI. Response matrix R for observable $\cos \theta_v$ for the muon mode. The bins are defined in Section VIII.

Bin	1	2	3	4	5	6	7	8	9	10
1	0.918	0.077	0.000	0.000	0.000	0.000	0.000	0.000	0.000	0.000
2	0.082	0.805	0.091	0.001	0.000	0.000	0.000	0.000	0.000	0.000
3	0.000	0.117	0.763	0.101	0.002	0.000	0.000	0.000	0.000	0.000
4	0.000	0.001	0.142	0.735	0.103	0.002	0.000	0.000	0.000	0.000
5	0.000	0.000	0.003	0.159	0.723	0.098	0.001	0.000	0.000	0.000
6	0.000	0.000	0.000	0.004	0.169	0.726	0.091	0.001	0.000	0.000
7	0.000	0.000	0.000	0.000	0.004	0.172	0.745	0.082	0.001	0.000
8	0.000	0.000	0.000	0.000	0.000	0.002	0.161	0.771	0.074	0.000
9	0.000	0.000	0.000	0.000	0.000	0.000	0.001	0.145	0.817	0.066
10	0.000	0.000	0.000	0.000	0.000	0.000	0.000	0.000	0.107	0.934

TABLE XXII. Response matrix R for observable χ for the muon mode. The bins are defined in Section VIII.

Bin	1	2	3	4	5	6	7	8	9	10
1	0.653	0.129	0.012	0.004	0.003	0.002	0.002	0.004	0.014	0.144
2	0.152	0.686	0.130	0.013	0.004	0.003	0.002	0.002	0.005	0.017
3	0.016	0.143	0.693	0.147	0.016	0.006	0.003	0.002	0.003	0.005
4	0.005	0.013	0.138	0.667	0.160	0.018	0.005	0.002	0.002	0.003
5	0.003	0.004	0.013	0.142	0.630	0.156	0.015	0.004	0.002	0.002
6	0.002	0.002	0.004	0.015	0.158	0.629	0.142	0.013	0.004	0.003
7	0.003	0.002	0.002	0.005	0.018	0.164	0.667	0.138	0.013	0.005
8	0.005	0.003	0.002	0.003	0.006	0.016	0.148	0.692	0.141	0.016
9	0.017	0.004	0.002	0.002	0.003	0.005	0.013	0.131	0.686	0.152
10	0.144	0.014	0.004	0.002	0.002	0.002	0.004	0.012	0.129	0.654

TABLE XXIII. Statistical uncertainty correlation matrix of $(w, \cos \theta_e)$ versus $(w, \cos \theta_\ell)$ for electron mode. The bins are defined in Section VIII.

TABLE XXIV. Statistical uncertainty correlation matrix of $(\cos \theta_v, \chi)$ versus $(w, \cos \theta_\ell)$ for the electron mode. The bins are defined in Section VIII.

Bin	21	22	23	24	25	26	27	28	29	30	31	32	33	34	35	36	37	38	39	40
1	0.022	0.009	0.002	-0.001	-0.003	-0.004	0.001	0.004	0.004	-0.003	0.005	0.012	0.019	0.017	0.015	0.007	-0.004	-0.026	-0.057	
2	0.019	0.021	0.013	0.006	0.001	-0.005	-0.003	-0.006	-0.004	0.000	0.003	0.006	0.007	0.006	0.004	0.002	-0.001	-0.007	-0.019	
3	0.017	0.027	0.018	0.006	0.001	0.004	-0.001	-0.007	-0.011	-0.015	0.005	0.002	-0.001	-0.004	-0.004	-0.004	-0.001	0.004	0.013	
4	0.015	0.028	0.024	0.018	0.009	0.001	-0.005	-0.012	-0.017	-0.020	0.008	0.002	-0.005	-0.010	-0.012	-0.012	-0.003	0.001	0.015	0.035
5	0.006	0.023	0.023	0.020	0.010	0.001	-0.003	-0.011	-0.019	-0.023	0.008	0.002	-0.007	-0.017	-0.016	-0.013	-0.008	0.005	0.021	0.046
6	-0.006	0.006	0.020	0.021	0.014	0.007	-0.001	-0.010	-0.018	-0.024	0.007	0.001	-0.009	-0.015	-0.019	-0.013	-0.008	0.004	0.020	0.051
7	-0.015	-0.008	0.008	0.016	0.011	0.007	-0.002	-0.001	-0.009	-0.017	0.000	-0.000	-0.007	-0.012	-0.013	-0.009	-0.004	0.004	0.015	0.031
8	-0.023	-0.029	-0.010	0.002	0.006	0.009	0.007	0.007	0.000	-0.004	-0.001	-0.002	-0.005	-0.005	-0.005	-0.001	-0.002	0.006	0.006	0.010
9	-0.024	-0.042	-0.038	-0.020	-0.004	0.005	0.014	0.023	0.019	0.010	-0.006	-0.004	-0.002	0.001	0.009	0.008	0.001	0.001	-0.006	-0.015
10	-0.026	-0.046	-0.054	-0.050	-0.024	-0.001	0.016	0.034	0.046	0.030	-0.011	-0.005	-0.001	0.011	0.015	0.015	0.006	0.001	-0.013	-0.040
11	-0.003	-0.004	-0.004	-0.001	0.000	0.005	0.001	0.003	-0.002	0.006	-0.003	0.000	0.001	-0.002	-0.002	-0.003	-0.004	-0.003	0.006	
12	0.001	0.004	0.001	0.005	0.000	0.001	-0.001	-0.002	-0.007	0.003	0.003	0.003	-0.000	-0.002	-0.000	-0.002	-0.002	-0.002	-0.001	
13	0.004	0.006	0.008	0.004	0.004	0.002	0.003	-0.002	-0.005	-0.009	0.002	0.001	0.002	0.001	-0.001	0.003	-0.001	0.000	-0.001	-0.002
14	0.003	0.001	0.006	0.005	0.002	0.001	-0.002	0.002	-0.001	-0.009	-0.003	-0.000	-0.004	-0.001	-0.002	-0.001	0.001	0.003	0.003	
15	-0.001	-0.002	0.003	0.001	0.000	0.002	-0.000	0.004	-0.003	-0.005	-0.006	-0.005	-0.005	-0.004	-0.003	-0.002	0.001	0.006	0.008	0.009
16	-0.001	0.001	-0.003	0.003	0.003	0.003	0.001	-0.001	-0.002	-0.004	-0.006	-0.003	-0.006	-0.006	-0.001	-0.000	0.002	0.006	0.008	0.011
17	0.000	0.004	0.004	0.003	0.003	0.004	0.003	-0.003	-0.002	-0.002	-0.008	-0.003	0.000	-0.002	-0.005	-0.000	0.002	0.004	0.005	0.003
18	0.007	0.006	0.006	0.009	0.004	0.002	0.000	-0.005	-0.004	-0.008	0.003	0.001	0.001	0.002	0.002	-0.001	-0.002	0.001	-0.005	
19	0.004	0.007	0.002	0.003	0.005	0.000	-0.001	0.002	-0.006	-0.008	0.005	0.003	0.003	-0.001	-0.000	-0.003	0.001	-0.004	-0.002	
20	-0.001	-0.006	-0.001	-0.003	-0.001	0.002	0.001	0.006	0.002	-0.005	0.006	0.002	0.000	-0.000	-0.004	-0.003	-0.003	0.001	0.001	

TABLE XXXV. Statistical uncertainty correlation matrix of $(w, \cos\theta_v, \chi)$ versus $(\cos\theta_v, \chi)$ for the electron mode. The bins are defined in Section VIII.

Bin	1	2	3	4	5	6	7	8	9	10	11	12	13	14	15	16	17	18	19	20
21	0.022	0.019	0.017	0.015	0.006	-0.006	-0.015	-0.023	-0.024	-0.026	-0.003	0.001	0.004	0.003	-0.001	0.000	0.007	0.004	-0.001	
22	0.009	0.021	0.027	0.028	0.023	0.006	-0.008	-0.029	-0.042	-0.046	-0.004	0.004	0.006	0.001	-0.002	0.001	0.004	0.006	0.007	-0.006
23	0.002	0.013	0.018	0.024	0.023	0.020	0.008	-0.010	-0.038	-0.054	-0.004	0.001	0.008	0.006	0.003	-0.003	0.004	0.006	0.006	-0.002
24	-0.001	0.006	0.006	0.018	0.020	0.021	0.016	0.002	-0.020	-0.050	-0.004	0.005	0.004	0.005	0.001	0.003	0.003	0.009	0.003	-0.003
25	-0.003	0.001	0.001	0.009	0.010	0.014	0.011	0.006	-0.004	-0.024	-0.001	0.000	0.004	0.002	0.000	0.003	0.003	0.004	0.005	-0.001
26	-0.004	-0.005	0.004	0.001	0.001	0.007	0.007	0.009	0.005	-0.001	0.000	0.001	0.002	0.001	0.002	0.003	0.004	0.002	0.000	0.002
27	-0.003	-0.003	-0.005	-0.005	-0.003	-0.001	-0.002	-0.007	0.014	0.016	0.005	-0.001	0.003	-0.002	-0.000	0.003	0.003	0.000	-0.001	0.001
28	0.001	-0.006	-0.007	-0.012	-0.011	-0.010	-0.001	0.007	0.023	0.034	0.001	0.001	-0.002	0.002	0.004	0.001	-0.002	-0.005	0.002	0.006
29	0.004	-0.006	-0.011	-0.017	-0.019	-0.018	-0.009	0.000	0.019	0.046	0.003	-0.002	-0.005	-0.001	-0.003	-0.002	-0.004	-0.006	-0.006	0.002
30	0.004	-0.004	-0.015	-0.020	-0.023	-0.024	-0.017	-0.004	0.010	0.030	-0.002	-0.007	-0.009	-0.009	-0.005	-0.004	-0.008	-0.008	-0.005	-0.005
31	-0.003	0.000	0.005	0.008	0.008	0.007	0.000	-0.001	-0.006	-0.011	0.005	0.004	0.002	-0.003	-0.006	-0.006	-0.003	0.003	0.005	0.006
32	0.005	0.003	0.002	0.002	0.000	0.001	-0.000	-0.002	-0.004	-0.005	0.003	0.003	0.002	-0.000	-0.005	-0.003	0.000	0.001	0.003	0.002
33	0.012	0.006	-0.001	-0.005	-0.007	-0.009	-0.007	-0.005	-0.002	-0.001	0.000	0.003	0.002	-0.004	-0.005	-0.006	-0.002	0.001	0.003	0.000
34	0.019	0.007	-0.004	-0.010	-0.017	-0.015	-0.012	-0.005	0.001	0.011	0.001	-0.000	0.001	-0.001	-0.004	-0.006	-0.005	0.001	-0.000	-0.000
35	0.017	0.006	-0.004	-0.012	-0.016	-0.019	-0.013	-0.005	0.009	0.015	-0.002	-0.002	-0.001	-0.002	-0.004	-0.001	-0.000	0.002	-0.000	-0.004
36	0.015	0.004	-0.004	-0.012	-0.013	-0.013	-0.009	-0.001	0.008	0.015	-0.002	-0.000	0.003	-0.001	-0.002	-0.000	-0.002	-0.000	-0.003	-0.003
37	0.007	0.002	-0.001	-0.003	-0.008	-0.008	-0.004	-0.002	0.001	0.006	-0.003	-0.002	-0.001	0.001	0.002	0.002	-0.001	-0.003	-0.003	-0.003
38	-0.004	-0.001	-0.001	0.005	0.004	0.004	0.006	0.001	0.001	-0.004	-0.002	0.000	0.003	0.006	0.004	-0.002	0.001	0.001	0.001	0.001
39	-0.026	-0.007	0.004	0.015	0.021	0.020	0.015	0.006	-0.006	-0.013	-0.003	-0.002	-0.001	0.003	0.008	0.005	0.001	-0.005	0.001	0.001
40	-0.057	-0.019	0.013	0.035	0.046	0.051	0.031	0.010	-0.015	-0.040	0.006	-0.001	-0.002	0.003	0.009	0.011	0.003	-0.005	-0.002	0.004

TABLE XXVII. Statistical correlation matrix of $(\cos \theta_v, \chi)$ versus $(\cos \theta_v, \chi)$ for the electron mode. The bins are defined in Section VIII.

TABLE XXVII. Statistical uncertainty correlation matrix of $(w, \cos\theta_\ell)$ versus $(w, \cos\theta_\ell)$ for the muon mode. The bins are defined in Section VIII.

TABLE XXVIII. Statistical uncertainty correlation matrix of $(\cos \theta_v, \chi)$ versus $(w, \cos \theta_\ell)$ for the muon mode. The bins are defined in Section VIII.

Bin	21	22	23	24	25	26	27	28	29	30	31	32	33	34	35	36	37	38	39	40
1	0.019	0.012	0.002	-0.001	-0.004	-0.005	0.000	0.001	0.003	0.001	-0.004	0.005	0.012	0.014	0.013	0.008	-0.001	-0.024	-0.051	
2	0.023	0.019	0.013	0.004	0.000	-0.002	-0.004	-0.006	-0.004	0.003	0.001	0.005	0.004	0.006	0.005	0.004	-0.000	-0.007	-0.019	
3	0.015	0.022	0.018	0.013	0.003	0.000	-0.005	-0.007	-0.012	-0.012	0.004	0.003	-0.001	-0.004	-0.005	-0.003	-0.002	0.003	0.007	
4	0.012	0.026	0.023	0.018	0.009	0.000	-0.005	-0.012	-0.018	-0.022	0.005	0.004	-0.005	-0.011	-0.014	-0.010	-0.007	0.002	0.015	
5	0.009	0.020	0.021	0.018	0.010	0.001	-0.005	-0.011	-0.020	-0.022	0.007	0.003	-0.008	-0.014	-0.016	-0.015	-0.009	0.006	0.023	
6	-0.006	0.011	0.021	0.017	0.014	0.006	-0.003	-0.011	-0.017	-0.022	0.004	0.000	-0.007	-0.014	-0.018	-0.013	-0.009	0.004	0.023	
7	-0.017	-0.009	0.006	0.012	0.014	0.008	0.001	-0.003	-0.011	-0.014	0.000	-0.001	-0.007	-0.009	-0.011	-0.009	-0.005	0.006	0.019	
8	-0.020	-0.024	-0.013	0.001	0.007	0.008	0.007	0.005	0.000	-0.007	-0.004	-0.003	-0.004	-0.005	-0.003	-0.002	0.001	0.002	0.008	
9	-0.023	-0.039	-0.035	-0.018	-0.004	0.007	0.014	0.020	0.017	0.010	-0.005	-0.004	-0.002	-0.000	0.004	0.006	0.005	0.003	-0.006	
10	-0.024	-0.043	-0.050	-0.042	-0.020	-0.003	0.017	0.033	0.039	0.032	-0.011	-0.009	-0.003	0.006	0.013	0.014	0.014	0.001	-0.013	
11	-0.002	-0.004	-0.003	-0.002	-0.001	0.004	0.003	0.002	-0.000	-0.006	0.009	0.000	-0.003	-0.003	-0.004	-0.003	-0.003	-0.001	0.008	
12	0.002	0.001	0.001	0.002	0.004	0.001	-0.001	-0.004	-0.005	-0.000	0.010	-0.001	-0.003	-0.002	0.001	0.000	-0.000	-0.002	-0.001	
13	0.006	0.004	0.006	0.006	0.001	0.002	-0.004	-0.004	-0.007	-0.000	0.000	0.006	-0.001	0.000	0.001	0.001	0.002	0.002	-0.006	
14	0.002	0.005	0.004	0.009	0.004	0.001	0.001	-0.002	-0.007	-0.008	-0.002	0.001	-0.002	0.002	-0.003	0.001	0.003	0.000	0.003	
15	-0.002	0.001	0.006	0.003	0.001	0.002	-0.001	-0.002	-0.005	-0.001	-0.005	-0.005	-0.008	-0.002	-0.003	0.000	0.005	0.013	0.010	
16	-0.002	0.000	-0.001	0.002	0.002	-0.002	0.003	-0.001	-0.005	-0.003	-0.005	-0.007	-0.007	0.001	0.002	0.005	0.009	0.013		
17	0.005	0.006	0.007	0.005	0.003	0.002	0.000	-0.002	-0.004	-0.008	-0.003	-0.002	-0.003	-0.003	0.001	0.006	0.004	0.002	0.005	
18	0.005	0.004	0.006	0.007	0.004	0.002	0.001	0.002	-0.005	-0.009	-0.001	0.001	0.002	-0.002	-0.001	0.000	0.008	0.002	-0.003	
19	0.002	0.006	0.002	-0.000	0.003	-0.001	0.002	-0.000	-0.003	-0.006	-0.000	0.002	-0.001	-0.002	0.000	-0.003	0.004	0.003	-0.003	
20	-0.003	-0.003	-0.005	-0.004	-0.000	0.001	0.003	0.003	0.002	-0.003	-0.001	0.001	-0.002	-0.002	-0.003	-0.004	-0.002	0.000	-0.001	

TABLE XXXIX. Statistical uncertainty correlation matrix of $(w, \cos\theta\ell)$ versus $(\cos\theta_b, \chi)$ for the muon mode. The bins are defined in Section VIII.

Bin	1	2	3	4	5	6	7	8	9	10	11	12	13	14	15	16	17	18	19	20
21	0.019	0.023	0.015	0.012	0.009	-0.006	-0.017	-0.020	-0.023	-0.024	-0.002	0.006	0.002	-0.002	0.005	0.005	0.005	0.002	-0.003	
22	0.012	0.019	0.022	0.026	0.020	0.011	-0.009	-0.024	-0.039	-0.043	-0.004	0.004	0.005	0.001	0.000	0.006	0.004	0.006	-0.003	
23	0.002	0.013	0.018	0.023	0.021	0.006	-0.013	-0.035	-0.050	-0.003	0.001	0.006	0.004	0.006	-0.000	0.007	0.006	0.002	-0.005	
24	-0.001	0.004	0.013	0.018	0.018	0.017	0.012	0.001	-0.018	-0.042	-0.002	0.002	0.006	0.009	0.003	0.001	0.005	0.007	-0.000	-0.004
25	-0.004	0.000	0.003	0.009	0.010	0.014	0.014	0.007	-0.004	-0.020	-0.001	0.002	0.006	0.004	0.001	0.002	0.003	0.004	0.003	-0.000
26	-0.005	-0.002	0.000	0.000	0.001	0.006	0.008	0.008	0.007	-0.003	0.004	0.004	0.001	0.001	0.002	0.002	0.002	-0.001	0.001	0.001
27	0.000	-0.004	-0.005	-0.005	-0.005	-0.003	0.001	0.007	0.014	0.017	0.003	0.001	0.002	0.001	-0.001	-0.002	0.000	0.001	0.002	0.003
28	0.001	-0.006	-0.007	-0.012	-0.011	-0.011	-0.003	0.005	0.020	0.033	0.002	-0.001	-0.004	-0.002	-0.001	0.003	-0.002	0.002	-0.000	0.003
29	0.003	-0.004	-0.012	-0.018	-0.020	-0.017	-0.011	0.000	0.017	0.039	-0.000	-0.004	-0.004	-0.007	-0.002	-0.001	-0.004	-0.005	-0.003	0.002
30	0.001	-0.004	-0.012	-0.022	-0.022	-0.014	-0.007	0.010	0.032	-0.006	-0.005	-0.007	-0.008	-0.005	-0.005	-0.008	-0.009	-0.006	-0.003	-0.003
31	-0.004	0.003	0.004	0.005	0.007	0.004	0.000	-0.004	-0.005	-0.011	0.000	0.001	0.001	-0.000	0.000	-0.001	-0.002	0.001	0.000	0.000
32	0.005	0.001	0.003	0.004	0.003	0.000	-0.001	-0.003	-0.004	-0.009	0.001	0.002	0.001	0.002	-0.004	-0.000	0.002	0.003	0.002	0.002
33	0.012	0.005	-0.001	-0.005	-0.008	-0.007	-0.007	-0.004	-0.002	-0.003	-0.002	0.001	0.001	-0.001	-0.004	-0.006	-0.002	0.003	0.000	0.001
34	0.014	0.004	-0.004	-0.011	-0.014	-0.014	-0.009	-0.005	-0.000	0.006	-0.002	-0.002	-0.000	-0.003	-0.007	-0.006	-0.002	-0.001	-0.001	-0.001
35	0.014	0.006	-0.005	-0.014	-0.016	-0.018	-0.011	-0.003	0.004	0.013	-0.003	-0.001	-0.001	-0.003	-0.006	-0.007	-0.003	-0.000	0.001	-0.002
36	0.013	0.005	-0.003	-0.010	-0.015	-0.013	-0.009	-0.002	0.006	0.014	-0.002	0.002	0.001	-0.002	-0.003	0.001	-0.000	0.000	-0.004	-0.004
37	0.008	0.004	-0.002	-0.007	-0.009	-0.005	-0.001	0.005	0.014	0.014	-0.003	0.001	0.001	0.003	0.001	0.001	0.001	-0.002	-0.001	-0.001
38	-0.001	-0.000	0.003	0.002	0.006	0.004	0.006	0.002	0.003	0.001	-0.001	0.000	0.002	0.000	0.005	0.005	0.002	0.004	0.000	0.000
39	-0.024	-0.007	0.007	0.015	0.023	0.019	0.023	0.023	0.019	0.002	-0.006	-0.013	0.001	-0.002	0.000	0.014	0.009	0.003	-0.004	-0.000
40	-0.051	-0.019	0.013	0.041	0.043	0.051	0.029	0.008	-0.016	-0.037	0.008	-0.001	-0.006	0.003	0.010	0.014	0.006	-0.003	-0.003	0.006

TABLE XXX. Statistical correlation matrix of $(\cos \theta_v, \chi)$ versus $(\cos \theta_v, \chi)$ for the muon mode. The bins are defined in Section VIII.

TABLE XXXI. Systematic uncertainty correlation matrix of $(w, \cos\theta_\ell)$ versus $(w, \cos\theta_\ell)$. The bins are defined in Section VIII.

Bin	1	2	3	4	5	6	7	8	9	10	11	12	13	14	15	16	17	18	19	20
1	1.000	0.872	0.755	0.682	0.656	0.612	0.555	0.500	0.487	0.409	0.786	0.699	0.633	0.621	0.623	0.628	0.630	0.640	0.653	0.662
2	0.872	1.000	0.955	0.899	0.878	0.850	0.819	0.779	0.763	0.680	0.934	0.891	0.855	0.857	0.865	0.872	0.877	0.879	0.889	0.896
3	0.755	0.955	1.000	0.978	0.957	0.936	0.917	0.891	0.885	0.819	0.952	0.946	0.933	0.943	0.951	0.957	0.957	0.963	0.969	0.974
4	0.682	0.899	0.978	1.000	0.985	0.967	0.952	0.943	0.931	0.854	0.934	0.950	0.952	0.959	0.968	0.977	0.979	0.984	0.986	0.990
5	0.656	0.878	0.957	0.985	1.000	0.992	0.978	0.950	0.941	0.875	0.925	0.957	0.968	0.980	0.986	0.987	0.989	0.990	0.993	0.992
6	0.612	0.850	0.936	0.967	0.992	1.000	0.994	0.963	0.948	0.879	0.906	0.950	0.970	0.982	0.987	0.986	0.988	0.987	0.989	0.985
7	0.555	0.819	0.917	0.952	0.978	0.994	1.000	0.979	0.967	0.902	0.884	0.938	0.967	0.982	0.987	0.986	0.986	0.982	0.983	0.976
8	0.500	0.779	0.891	0.943	0.950	0.963	0.979	1.000	0.991	0.922	0.858	0.918	0.951	0.963	0.969	0.973	0.971	0.968	0.963	0.956
9	0.487	0.763	0.885	0.931	0.941	0.948	0.967	0.991	1.000	0.961	0.838	0.904	0.941	0.965	0.971	0.973	0.969	0.965	0.958	0.951
10	0.409	0.680	0.819	0.854	0.875	0.879	0.902	0.922	0.961	1.000	0.755	0.840	0.885	0.928	0.929	0.922	0.912	0.905	0.896	0.887
11	0.786	0.934	0.952	0.934	0.925	0.906	0.884	0.858	0.838	0.755	1.000	0.983	0.952	0.927	0.915	0.906	0.902	0.907	0.918	0.919
12	0.699	0.891	0.946	0.950	0.957	0.950	0.938	0.918	0.904	0.840	0.983	1.000	0.991	0.972	0.959	0.947	0.941	0.941	0.945	0.945
13	0.633	0.855	0.933	0.952	0.968	0.970	0.967	0.951	0.941	0.885	0.952	0.991	1.000	0.989	0.978	0.966	0.961	0.958	0.964	0.956
14	0.621	0.857	0.943	0.959	0.980	0.982	0.982	0.963	0.965	0.928	0.927	0.972	0.989	1.000	0.997	0.989	0.984	0.981	0.983	0.977
15	0.623	0.865	0.951	0.968	0.986	0.987	0.987	0.969	0.971	0.929	0.915	0.959	0.978	0.997	1.000	0.997	0.994	0.992	0.993	0.988
16	0.628	0.872	0.957	0.977	0.987	0.986	0.973	0.973	0.922	0.906	0.947	0.966	0.989	0.997	1.000	0.999	0.998	0.997	0.995	0.995
17	0.630	0.872	0.957	0.979	0.989	0.988	0.986	0.971	0.969	0.912	0.902	0.941	0.961	0.984	0.994	0.999	1.000	0.999	0.996	0.996
18	0.640	0.879	0.963	0.984	0.990	0.987	0.982	0.968	0.965	0.905	0.907	0.941	0.958	0.981	0.992	0.998	0.999	1.000	0.999	0.998
19	0.653	0.889	0.969	0.986	0.993	0.989	0.983	0.963	0.958	0.896	0.918	0.964	0.983	0.993	0.997	0.999	0.999	1.000	0.999	0.999
20	0.662	0.896	0.974	0.990	0.992	0.985	0.976	0.956	0.951	0.887	0.919	0.945	0.956	0.977	0.988	0.995	0.996	0.998	0.999	1.000

TABLE XXXII. Systematic correlation matrix $(\cos \theta_v, \chi)$ and $(w, \cos \theta_\ell)$ distribution. The bins are defined in Section VIII.

Bin	21	22	23	24	25	26	27	28	29	30	31	32	33	34	35	36	37	38	39	40
1	0.508	0.763	0.877	0.919	0.954	0.970	0.983	0.975	0.981	0.951	0.851	0.920	0.958	0.980	0.981	0.974	0.970	0.964	0.961	0.950
2	0.524	0.783	0.895	0.938	0.967	0.981	0.991	0.982	0.983	0.942	0.866	0.930	0.964	0.984	0.987	0.983	0.980	0.976	0.973	0.964
3	0.558	0.814	0.921	0.963	0.983	0.990	0.994	0.986	0.981	0.926	0.886	0.941	0.968	0.985	0.991	0.991	0.991	0.988	0.987	0.981
4	0.591	0.842	0.942	0.982	0.991	0.991	0.989	0.980	0.969	0.901	0.902	0.947	0.968	0.980	0.987	0.991	0.993	0.992	0.992	0.990
5	0.638	0.880	0.967	0.992	0.990	0.981	0.973	0.965	0.958	0.896	0.918	0.950	0.961	0.977	0.985	0.992	0.993	0.995	0.995	0.996
6	0.686	0.911	0.984	0.996	0.988	0.973	0.960	0.945	0.938	0.873	0.934	0.953	0.957	0.971	0.979	0.986	0.988	0.991	0.993	0.996
7	0.731	0.938	0.993	0.991	0.982	0.964	0.946	0.922	0.916	0.848	0.944	0.953	0.950	0.963	0.972	0.978	0.980	0.984	0.987	0.991
8	0.756	0.952	0.997	0.979	0.968	0.947	0.928	0.898	0.897	0.840	0.949	0.941	0.956	0.963	0.967	0.972	0.976	0.976	0.981	
9	0.781	0.965	0.996	0.968	0.956	0.936	0.915	0.879	0.873	0.806	0.954	0.947	0.934	0.943	0.949	0.952	0.953	0.957	0.964	0.968
10	0.840	0.993	0.976	0.925	0.912	0.887	0.861	0.816	0.806	0.739	0.947	0.920	0.894	0.900	0.905	0.907	0.912	0.912	0.922	0.927
11	0.666	0.900	0.974	0.989	0.991	0.984	0.977	0.962	0.955	0.891	0.926	0.956	0.968	0.982	0.991	0.995	0.996	0.997	0.998	
12	0.668	0.900	0.975	0.989	0.992	0.985	0.978	0.962	0.957	0.897	0.931	0.960	0.971	0.986	0.993	0.996	0.997	0.999	0.998	
13	0.651	0.886	0.965	0.981	0.993	0.991	0.986	0.965	0.961	0.904	0.928	0.963	0.978	0.992	0.997	0.997	0.996	0.998	0.995	
14	0.633	0.869	0.955	0.975	0.990	0.990	0.988	0.971	0.970	0.919	0.922	0.962	0.978	0.995	0.999	0.998	0.996	0.995	0.995	0.992
15	0.608	0.849	0.942	0.968	0.987	0.990	0.991	0.974	0.975	0.926	0.906	0.951	0.972	0.993	0.998	0.997	0.995	0.994	0.993	0.989
16	0.609	0.851	0.944	0.970	0.987	0.991	0.992	0.977	0.976	0.924	0.908	0.952	0.973	0.992	0.998	0.997	0.996	0.994	0.990	
17	0.634	0.871	0.957	0.978	0.992	0.992	0.989	0.969	0.966	0.911	0.917	0.955	0.972	0.991	0.997	0.998	0.998	0.997	0.998	0.995
18	0.657	0.890	0.969	0.985	0.990	0.986	0.981	0.968	0.964	0.908	0.930	0.962	0.974	0.990	0.995	0.998	0.998	0.997	0.998	0.996
19	0.670	0.902	0.975	0.985	0.990	0.984	0.977	0.960	0.957	0.903	0.935	0.964	0.974	0.990	0.995	0.996	0.995	0.997	0.996	
20	0.665	0.899	0.974	0.989	0.990	0.984	0.977	0.963	0.956	0.926	0.956	0.969	0.983	0.991	0.995	0.996	0.996	0.998	0.998	

TABLE XXXIII. Systematic correlation matrix ($w, \cos\theta_v, \chi$) and ($\cos\theta_v, \chi$) distributions. The label for each bin is defined in Section VIII.

Bin	1	2	3	4	5	6	7	8	9	10	11	12	13	14	15	16	17	18	19	20
21	0.508	0.524	0.558	0.591	0.638	0.686	0.731	0.756	0.781	0.840	0.666	0.651	0.633	0.608	0.609	0.634	0.657	0.670	0.665	
22	0.763	0.783	0.814	0.842	0.880	0.911	0.938	0.952	0.965	0.993	0.900	0.886	0.869	0.849	0.851	0.871	0.890	0.902	0.899	
23	0.877	0.895	0.921	0.942	0.967	0.984	0.993	0.997	0.996	0.976	0.974	0.975	0.965	0.955	0.942	0.944	0.957	0.969	0.975	
24	0.919	0.938	0.963	0.982	0.992	0.996	0.991	0.979	0.968	0.925	0.989	0.981	0.975	0.968	0.970	0.978	0.985	0.985	0.989	
25	0.954	0.967	0.983	0.991	0.990	0.988	0.982	0.968	0.956	0.912	0.991	0.992	0.993	0.990	0.987	0.987	0.992	0.990	0.990	
26	0.970	0.981	0.990	0.991	0.981	0.973	0.964	0.947	0.936	0.887	0.984	0.985	0.991	0.990	0.991	0.992	0.992	0.986	0.984	
27	0.983	0.991	0.994	0.989	0.973	0.960	0.946	0.928	0.915	0.861	0.977	0.978	0.986	0.988	0.991	0.992	0.989	0.981	0.977	
28	0.975	0.982	0.986	0.980	0.965	0.945	0.922	0.898	0.879	0.816	0.962	0.965	0.971	0.974	0.977	0.977	0.969	0.968	0.963	
29	0.981	0.983	0.981	0.969	0.958	0.938	0.916	0.897	0.873	0.806	0.955	0.957	0.961	0.970	0.975	0.976	0.966	0.964	0.957	
30	0.951	0.942	0.926	0.901	0.896	0.873	0.848	0.840	0.806	0.739	0.891	0.897	0.904	0.919	0.926	0.924	0.911	0.908	0.903	
31	0.851	0.866	0.886	0.902	0.918	0.934	0.944	0.949	0.954	0.947	0.926	0.931	0.928	0.922	0.906	0.908	0.917	0.930	0.935	
32	0.920	0.930	0.941	0.947	0.950	0.953	0.949	0.947	0.920	0.956	0.960	0.963	0.962	0.951	0.952	0.955	0.962	0.964	0.956	
33	0.958	0.964	0.968	0.968	0.961	0.957	0.950	0.941	0.934	0.894	0.968	0.971	0.978	0.972	0.973	0.972	0.974	0.974	0.969	
34	0.980	0.984	0.985	0.980	0.977	0.971	0.963	0.956	0.943	0.900	0.982	0.986	0.992	0.995	0.993	0.992	0.991	0.990	0.983	
35	0.981	0.987	0.991	0.987	0.985	0.979	0.972	0.963	0.949	0.905	0.991	0.993	0.997	0.999	0.998	0.998	0.997	0.995	0.991	
36	0.974	0.983	0.991	0.991	0.992	0.986	0.978	0.967	0.952	0.907	0.995	0.996	0.997	0.998	0.997	0.998	0.998	0.996	0.995	
37	0.970	0.980	0.991	0.993	0.993	0.988	0.980	0.967	0.953	0.907	0.996	0.996	0.997	0.995	0.996	0.996	0.997	0.995	0.996	
38	0.964	0.976	0.988	0.992	0.995	0.991	0.984	0.972	0.957	0.912	0.997	0.997	0.996	0.994	0.994	0.997	0.997	0.996	0.996	
39	0.961	0.973	0.987	0.992	0.995	0.993	0.987	0.976	0.964	0.922	0.998	0.999	0.998	0.995	0.993	0.994	0.998	0.997	0.998	
40	0.950	0.964	0.981	0.990	0.996	0.991	0.981	0.968	0.927	0.997	0.998	0.995	0.992	0.989	0.990	0.995	0.996	0.996	0.996	

TABLE XXXIV. Systematic uncertainty correlation matrix between $(\cos \theta_v, \chi)$ and $(\cos \theta_v, \chi)$ distribution. The bins are defined in Section VIII.

Bin	21	22	23	24	25	26	27	28	29	30	31	32	33	34	35	36	37	38	39	40
21	1.000	0.998	0.987	0.968	0.949	0.929	0.911	0.894	0.873	0.813	0.953	0.957	0.969	0.978	0.985	0.984	0.975	0.964	0.959	0.954
22	0.998	1.000	0.995	0.981	0.964	0.946	0.928	0.910	0.890	0.830	0.966	0.969	0.979	0.986	0.991	0.991	0.985	0.975	0.970	0.966
23	0.987	0.995	1.000	0.995	0.983	0.968	0.952	0.933	0.914	0.855	0.981	0.983	0.989	0.993	0.995	0.996	0.992	0.987	0.982	0.981
24	0.968	0.981	0.995	1.000	0.994	0.984	0.970	0.950	0.934	0.878	0.990	0.990	0.991	0.991	0.991	0.992	0.992	0.991	0.988	0.990
25	0.949	0.964	0.983	0.994	1.000	0.996	0.987	0.974	0.959	0.912	0.995	0.995	0.992	0.990	0.986	0.987	0.990	0.995	0.994	0.995
26	0.929	0.946	0.968	0.984	0.996	1.000	0.997	0.988	0.978	0.939	0.995	0.995	0.989	0.984	0.977	0.978	0.986	0.993	0.994	0.995
27	0.911	0.928	0.952	0.970	0.987	0.997	1.000	0.996	0.991	0.962	0.991	0.991	0.983	0.976	0.967	0.968	0.978	0.986	0.990	0.991
28	0.894	0.910	0.933	0.950	0.974	0.988	0.996	1.000	0.996	0.976	0.980	0.981	0.974	0.966	0.955	0.955	0.967	0.977	0.982	0.980
29	0.873	0.890	0.914	0.934	0.959	0.978	0.991	0.996	1.000	0.986	0.971	0.971	0.963	0.952	0.939	0.939	0.953	0.964	0.972	0.971
30	0.853	0.830	0.855	0.878	0.912	0.939	0.962	0.976	0.986	1.000	0.931	0.931	0.921	0.907	0.889	0.890	0.908	0.923	0.934	0.931
31	0.953	0.966	0.981	0.990	0.995	0.991	0.980	0.971	0.931	1.000	0.999	0.997	0.993	0.988	0.989	0.994	0.997	0.998	1.000	
32	0.957	0.969	0.983	0.990	0.995	0.991	0.981	0.971	0.931	0.999	1.000	0.998	0.995	0.991	0.992	0.996	0.999	0.999	0.999	
33	0.969	0.979	0.989	0.991	0.992	0.989	0.983	0.974	0.963	0.921	0.997	0.998	1.000	0.999	0.996	0.999	0.998	0.998	0.997	
34	0.978	0.986	0.993	0.991	0.990	0.984	0.976	0.966	0.952	0.907	0.993	0.995	0.999	1.000	0.999	0.999	0.997	0.996	0.996	
35	0.985	0.991	0.995	0.991	0.986	0.977	0.967	0.955	0.939	0.889	0.988	0.991	0.996	0.999	1.000	1.000	0.998	0.994	0.992	
36	0.984	0.991	0.996	0.992	0.987	0.978	0.968	0.955	0.939	0.890	0.989	0.992	0.996	0.999	1.000	1.000	0.998	0.995	0.993	
37	0.975	0.985	0.992	0.992	0.990	0.986	0.978	0.967	0.953	0.908	0.994	0.996	0.999	0.998	1.000	1.000	0.997	0.996	0.994	
38	0.964	0.975	0.987	0.991	0.995	0.986	0.977	0.964	0.923	0.997	0.999	0.998	0.997	0.994	0.995	0.997	1.000	0.999	0.997	
39	0.959	0.970	0.982	0.988	0.994	0.990	0.982	0.972	0.934	0.998	0.999	0.998	0.996	0.992	0.993	0.996	0.999	1.000	0.998	
40	0.954	0.966	0.981	0.990	0.995	0.991	0.980	0.971	0.931	1.000	0.999	0.997	0.993	0.988	0.989	0.994	0.997	0.998	1.000	